ARDHI UNIVERSITY

ASSESSING SPATIAL-TEMPORAL DYNAMICS OF MSIMBAZI BASIN GEOMORPHOMETRY

SULEIMAN RAHMA YUSSUF

BSc. Geoinformatics

Dissertation

Ardhi University, Dar es Salaam

July, 2023

ASSESSING SPATIAL-TEMPORAL DYNAMICS OF MSIMBAZI BASIN GEOMORPHOMETRY

SULEIMAN, RAHMA YUSSUF

A Dissertation Submitted to the Department of Geospatial Sciences and Technology in Partially Fulfilment of the Requirements for the Award of a Bachelor of Science in Geoinformatics (BSc. GI) of Ardhi University

CERTIFICATION

The undersigned certify that they have read and hereby recommend for acceptance by the Ardhi University dissertation titled "**Assessing Spatial Temporal Dynamics of Msimbazi Basin Geomorphometry"** in partial fulfillment of the requirements for the award of degree of Bachelor of Science in Geoinformatics at Ardhi University.

……..……. ….…….

Dr. Zakaria Ngereja

(Main Supervisor)

Ms. Beatrice Kaijage

(Second Supervisor)

Date…… Date……

DECLARATION AND COPYRIGHT

I Suleiman, Rahma Yussuf hereby declare that, the contents of this dissertation are the results of my own findings through my study and investigation, and to the best of my knowledge they have not been presented anywhere else as a dissertation for diploma, degree or any similar academic award in any institution of higher learning.

……..

SULEIMAN, RAHMA YUSSUF

(22745/T.2019)

ACKNOWLEDGEMENT

First and foremost, I would like to give my sincere thanks to Almighty God for the protection, good health, knowledge, strength and ability toward accomplishment of my dissertation work.

Furthermore, this research would have not been possible without the guidance, assistant and help from several individuals who played great roles for support in different ways.

Moreover, I would like to give my special thanks to my supervisors for their scientific, technical, professional discussion, advices, encouragements, guidelines and time for reviewing my work with great care and proving many helpful comments that further have made my dissertation improved and successfully completed

I would also like to give my thanks to all academic staffs of Department of Geospatial Sciences and Technology (DGST) for their guidance, hospitality and for creating a friendly and conducive environment which helped in making my social as well as professional experiences delightful at Ardhi University.

Also, I would like to thank my colleagues for their support within my year of study.

Finally, more thanks go to my family for their encouragements, guidance, patience, care and assistance throughout the years of my studies.

DEDICATION

I would like to dedicate this research to my parents who instilled within me the desire to learn and fought through thick and thin and made sacrifices so as for me to have access to a quality of education. Also, I dedicate this research to my whole family for giving me the support I required. Moreover, I would like to dedicate this research to my friends who supported me through my whole journey of studying.

ABSTRACT

Most river catchments around the world, which appear to be in towns face the problem of encroachment. About large population of the town tend to settle along the river. The same problem as in Dar es salaam Tanzania whereby the Msimbazi basin is currently occupied by a large number of settlements. People living along the Msimbazi basin heavily impact the ecology and geomorphology of the area in such a way the frequency of flash floods at recent years has increased compared to the previous years where the settlement along it was less. This study aimed to understand how the spatial and temporal dynamics occurring along the Msimbazi basin greatly affect the geomorphometry of the area and consequently how this effect link with recent cases of flash floods for the study year 1995, 2009 and 2022.

The methodology of this research consists of three chronological steps. The first step was about LULC classification using optical data sets and the two polarization bands from radar dataset, the second step was about generation of DTM for the year 2009 using Sentinel-1 toolbox since it was not readily available followed by extraction of terrain parameters for year 1995, 2009 and2022. The third step was about generation of landform map using eCognition software. Knowledge-based rules were used to assign the morphometric regions to their respective landform. A total of 15 landforms from Wood (1996) and Dikau (1989) were generated.

The results showed that as the time goes by from 1995 to 2022, the settlement along the basin tend to increase. The increase is not only seen in the landcover only, as well as the landforms were changing. It could be noted that with the increase of settlement, there was a decrease in the number of landforms and hence show relationship of population increase with geomorphometry.

TABLE OF CONTENTS

LIST OF FIGURES

LIST OF TABLES

ACRONYMS AND ABBREVIATIONS

DEM	Digital Elevation Model
DN	Digital Number
DTM	Digital Terrain Model
GIS	Geographic Information Systems
InSAR	Interferometric Synthetic Aperture Radar
ISODATA	Iterative Self-Organizing Data Analysis Technique
LCCS	Land Cover Classification Scheme
LULC	Land Use Land Cover
NASA	National Aeronautics and Space Administration
NBS	National Bureau of Standards
OBIA	Object Based Image Analysis
OLI	Operational Land Imager
SAR	Synthetic Aperture Radar
SLC	Single Look Complex
SRTM	Shuttle Radar Topography mission
TM	Thematic Mapper
USGS	United States Geological Survey
UTM	Universal Transverse Mercator

CHAPTER ONE

INTRODUCTION

1.0 Background

Globally, across developing countries, rivers in urban areas tend to be severely degraded in terms of ecology and morphology compared to their rural counterparts (Gurnell et al., 2007). Kunzig (2011) illustrates that, population increase in urban areas is among the contributing factors whereby currently half of the global population is living in urban areas. The basins containing rivers and wetlands are very significant to the surrounding dwellers in various ways, altogether aiming at boosting the economy for most developing countries but unfortunately, the benefits are frequently overlooked and lead to basin mismanagement and degradation posed by increasing population (Machiwa et al., 2021). Furthermore, the increase of population leads to the increase of human activities that result in variation of land use and ultimately land cover changes (Machiwa et al., 2021).

Population growth implies that vast development tends to occur in an area whereby numerous activities are being carried out on land. Considering Tanzania as a country whose cities are trending in urbanization due to favorable geographical location, industrialization and rapid population growth (Kebede & Nicholls, 2012). Dar es salaam city being among those cities has an alarming population growth and is showing high rate of urbanization compared to the other regions as seen from the census reports derived from National Bureau of Standards (NBS). This is because the city has developed in several aspects such as industrialization, employment opportunities and large market which is found to be higher compared to other regions/cities in Tanzania.

About 15% of Dar es salaam city coverage is occupied by a basin known as Msimbazi basin (Igulu & Mshiu, 2020). The Msimbazi Basin in Dar es Salaam is a strategically important area for infrastructure, mobility, commerce and ecosystem services including flood control (PO-RALG, 2021). Communities living at the lower reaches of the river, which are poor, unplanned settlements, largely depend on close access to Dar es Salaam's central business district for their livelihoods, and benefit from social services within walking distance (PO-RALG, 2021).

The area along the Msimbazi watershed was identified as hazardous in the 1979 Dar es Salaam city master plan (Armstrong, 1987), but yet people are still living along it. Hazard is conceived as a potentially damaging physical event, phenomenon or human activity, which may cause the loss of life or injury, property-damage, social and economic disruption or environmental degradation to the extent of leading to a disaster (Kironde, 2016). Within a catchment area, when human activities are carried out arbitrarily, tend to exert pressure on the resource and hence it leads into adverse impact on rivers and wetlands, such as land degradation, soil erosion, biodiversity loss, pollution and frequent floods (Kalisa et al., 2013). This is possible due to the fact that, it tends to increase of surface runoff volume, peak discharge and decrease of groundwater discharge (Igulu & Mshiu, 2020). In the case of Msimbazi basin, frequent flood events have been occurring that

endanger the lives of community living around it, their properties as well as infrastructure available in the area. One among the reasons that contribute to the cases of flooding is by blocking of natural drainage, which is caused by invading or making industrial developments on reclaimed wetlands where floodwater used to drain as reported by respondents from Bonde la Mpunga (Douglas et al., 2008).

According to Woodhouse (2018), the Dar-es-salaam city including Msimbazi basin is underlain by loose, sandy and loamy soils, which are very susceptible to erosion. As it is also known that urbanization plays a significant role in deforestation and soil erosion (Utepov et al., 2020), this is because vegetation holds the soil but when this relationship is interacted, the soil can be eroded easily and as well as the surface water runoff increase in velocity and quantity and consequently flood. This makes the city in a danger of flood.

Accurate prediction of flood is complex as a whole worldwide. Therefore, recognition of the patterns of flood is essential since it provide an insight into its nature and its characteristics which may aid into the generation of preventive measures of combating it. The major effects of floods are the morphometric changes caused by sedimentation and erosion. As stated by (Woodhouse, 2018) erosion as well as sedimentation as being morphological process which affects river processes and flood risk within Tanzania's largest city. Sedimentation and soil erosion are among the building factor of many landforms such as plains, hills, mountains, valleys and other small landforms.

The recognition of these landforms is a complex phenome. However, with the advances of Geographic Information Systems (GIS), the availability of DEMs and advance of technology and digital image processing techniques, has simplified the extraction of landforms. Automatic recognition of landforms technique, mostly requires the generation of land surface parameters from DEM which serves as input to the classification of landforms.

Landforms influence the surface flow, sediment transport and deposition, soil production, vegetation distribution and climate on local and regional scale (Straumann, 2010). Therefore, understanding of flood through the use of morphometric information may be an effective way of getting useful information about floods. Accurate recognition of landforms and its effective utilization can advance the development of many fields ranging from environmental research to socio-economic issues. Due to the recent flash floods happened along Msimbazi basin in 2015, we can understand the fact that change of Land Use/Land Cover (LULC) may aid to the change of the morphometry of the terrain and consequently change of water behavior on land. This study aims at understanding the pattern existing between the LULC change and the geomorphometry existing at the basin on addressing the recent flash floods occurring at the basin

1.1 Statement of the problem

Understanding well the factors contributing to the occurrence of floods and inundation extent is an important thing in the management of flood (Kibugu et al., 2022). The deviation of the behavior

of a river is primarily affected by activities carried out around it such that the change introduced by these activities result to a land cover change, which subsequently change the flow or river thus leading to frequent floods. Several studies have proved this including the study by Machiwa et al (2021) which dealt with the "Monitoring the Spatial Temporal Dynamics of LULC in the Msimbazi Basin, Tanzania", the study by Igulu & Mshiu (2020) which aimed at "Monitoring Impervious Surface Area Dynamics to Assess Urbanization of a Catchment" and as well as many other studies carried out showcasing the Msimbazi Basin plus studies carried outside the Msimbazi river. These researches seem to concluded that the morphometry of the basin is changing and that this change is brought by two interpretation thoughts, some concluded that the morphometric parameters are changing while others concluded that there seems to be erosion and sedimentation. Although these studies highlighted these effects, yet the degree, amount or rate of morphometric change is not understood. The main aim of this research is to quantitatively determine if there is correlation between LULC change and the geomorphometry of the river and if it there is, at what rate and as well as establishing a link on frequent cases of flash floods.

1.2 Research objectives

In this study there were two objectives, the main objective provides a general view of a research and specific objectives provide essential information on the exact goal performed.

1.2.1 Main objective

To assess the spatial-temporal dynamics of Msimbazi river basin geomorphometry.

1.2.2 Specific objectives

- Analysis of the Land Cover changes which took place at Msimbazi basin which took place from 1995 to 2022.
- Analysis of the change of the land surface parameters which took place at the period 1995, 2009 and 2022.
- Analysis of the dynamics of landforms from 1995-2022.
- Analysis of the relation between LULC changes with respect to landform changes.

1.3 Significance of the research

This study is significant to researchers, scientists and government as it enables them to better understand the processes and changes that are happening within a basin. This is due to the fact that the information derived regarding this field can be used to identify potential issues, such as erosion or sediment buildup, and develop strategies to manage and protect the river basin. Also, this study provides valuable insight into the history and evolution of the landscape and as well as help researchers predict how it may change in the future.

1.4 Scope and limitation

This research covers the assessment of spatial-temporal dynamics of Msimbazi basin geomorphometry basically in a sense of extraction of landforms with the use of remote sensing application and GIS approaches.

CHAPTER TWO

LITERATURE REVIEW

2.0 Overview

This chapter provides an insight to the basic terms and information on what the research is about.

2.1 Remote sensing overview

Remote sensing is the science of obtaining reliable information about the properties of surfaces and objects from distance, typically from aircraft or satellites, without physical contact with the objects, and of analyzing and interpreting images for deriving information about the earth's land and water areas (Boussema, 2017). Remote sensing by so far is a major source of information to several fields such as weather, forestry, agriculture, surface changes and biodiversity. However, derived datasets from any observation processes require preprocessing as there are no exact measurements in any observation.

2.2.1 Image pre processing

Image preprocessing by definition are the steps taken to format images before they are used by model training and inference (Nelson, 2020). However, these operations do not increase image information content but they decrease it if entropy is an information measure. The purpose of pre-processing is to raise the image's quality so that we can analyze it more effectively. Preprocessing allows us to eliminate unwanted distortions and improve specific qualities that are essential for the application we are working on. Those characteristics could change depending on the application (Kumar, 2021).

When image is distorted, it may produce radiometric error and as well as geometric error.

1. Radiometric error

Error induced affecting the measured brightness values of the pixels. It can be classified into internal error and external error. A process that improves the quality and accuracy of remote sensing images by removing or reducing the effects of atmospheric, sensor, and illumination factors is known as radiometric correction

2. Geometric error

Error induced affecting the position of DN values such as distance, area, direction and shape properties vary across the image. The process of correcting these distortions and assigning the properties (and practical value) of a map to an image is known as geometric correction.

2.2.2 Radar image pre processing

Due to the coherent nature of the sensor, standard image processing techniques are not applicable to radar images. Therefore, there is a need to develop preprocessing techniques for radar images which will then allow these standard methods to be applied (Frost et al., 1980). Radar images are subjected to many distortions such as image foreshortening, noise, layover and many others.

2.1.2.1 Radar

The short form of radar is Radio Detection and Ranging. It is a ranging or distance measuring device (fundamentals of remote sensing tutorial reference). It is an active remote sensing technique and can capture information in all-day as well as in unfavorable weather conditions, but could not provide spectral information, resulting in difficulties in image interpretation

Examples of radar dataset.

Table 2-1: Examples of radar datasets

S/N	Satellite	Band	Agency	Period
1	Seasat	L	US DoD	1978
2	ERS-1	C	ESA	1992–1996
3	JERS-1	L	JAXA	1992–1998
4	RADARSAT-1	C	CSA	1995–2013
5	ERS-2	C	ESA	1996–2011
6	SRTM	C, X	NASA	2000
7	ENVISAT	C	ESA	2002–2011
8	ALOS	L	JAXA	2006–2011
9	RADARSAT-2	C	CSA	2007–present
10	TerraSAR-X	X	DLR	2007–present
11	COSMO-SkyMed	X	ASI	2007–present
12	TanDEM-X	X	DLR	2010–present
13	ALOS-2	L	JAXA	2014–present
14	Sentinel-1	C	ESA	2014–present

15	SAOCOM	L	CONAE/ASI	2017–present
16	NISAR	L	NASA/ISRO	2021 (planned)
17	ALOS-4	L	JAXA	2022 (planned)
18	Tandem-L	L	DLR	(planned)

Consider Sentinel-1 SAR.

Acquisition mode

- Extra wide swath (WS) (for monitoring oceans and coasts)
- Strip mode (SM) (special orders only)
- Wave mode (WM) (routine collection for the ocean)
- Interferometric wide swath (IW) (routine collection for land) (5m by 20m)

Types of products

- Single look complex (SLC)
- Ground range detected (GRD)
- OCN

Note: Sentinel-1 satellite images in Interferometric Wide (IW) swath mode at level 1 with Ground Range Detection (GRD) are widely used to identify the Land Cover (Marrakchi et al., 2021).

SAR dataset can be used in delineating DEMs as well as for mapping landcover. For landcover preparation, the type of product used is ground range detected (GRD) while for generation of DEMs, single look complex (SLC) is opted. SAR images taken from L-band satellites complement satellites at shorter wavelengths such as C- and X-bands. L-band SAR has lower resolution than C- and X-band images but are more coherent over time, especially in vegetated regions (VV polarization is good for identifying the area of the flood (water bodies and land) while VH polarization is good for differentiating agricultural land and forest land)

2.1.2.2 Radiometric correction

Below are some of the radiometric corrections which are applied to the SAR dataset.

- Calibration

It involves the conversion of the signal recorded by the sensor in the form of digital accounts into backscatter coefficient (Marrakchi et al., 2021). It is essential as it creates an image where the value of each pixel is directly related to the backscatter of the surface.

- Thermal noise removal

It is a fundamental step for a precise radiometric calibration of synthetic aperture radar (SAR) data (Mascolo et al., 2021). This is done required to normalize the backscatter signal within the entire SAR image and is applied to remove noise from the channel intensities.

- Speckle filtering

Speckle appears as a grainy "salt and pepper" texture in an image. This is caused by random constructive and destructive interference from the multiple scattering returns that will occur within each resolution cell (Barton & Leonov, 1997). It corrupts information about the surface Speckle problem in an image is preprocessed using multiple looks. by increasing the o of looks It influences the azimuth resolution although it improves the interpretability of an image.

2.1.2.3 Geometric correction

- Geometric terrain correction

Geometric terrain correction (georeferencing) permits to correct the geometric distortions by using the Digital Elevation Model (DEM) proposed by the NASA's Shuttle Radar Topography Mission (SRTM) (Marrakchi et al., 2021)

2.2.3 Image classification

Image classification is the process of assigning land cover classes to pixels. For example, classes include water, urban, forest, agriculture and grassland (Dimyati et al., 1996). It can be broadly defined as the process of categorizing all pixels in an image or raw remotely sensed satellite data to obtain a given set of labels or land cover themes (Lillesand & Keifer, 1994). Classification process is performed in order to produce LULC maps which can aid in the process of decision making regarding different application such as evaluation, monitoring as well as analysis concerning certain phenomena. Therefore, more simplified information can be presented. Image classification consist of three main techniques. These are;

- Unsupervised image classification
- Supervised image classification
- Object-based image analysis (OBIA)

The higher the spatial resolution of the image the more sophisticated classification technique and vice versa. Hence when the image is having a high spatial resolution such as 5m, it is best to opt for (OBIA).

1. Unsupervised classification:

In this technique the analyst requests the computer to examine the image and extract a number of spectrally distinct clusters. The classification process which includes the grouping of clusters is

conducted by the computer machine without the human interaction. The analyst work is to select the numbers of classes and later on, to manually assign those clusters to their respective class.

2. Supervised classification:

Analyst identifies training sites to represent in classes and each pixel is classified based on statistical analysis. It involves more of human interaction.

Note: Before performing classification, the quality of the training samples should first be checked. The process itself is known as separability analysis. The term separability analysis refers to a test applied to the training samples to determine how distinct the classes are.

Examples of classification algorithm in supervised classification

- Maximum likelihood
- Minimum-distance
- Principal components
- Support vector machine (SVM)
- Iso cluster
- Artificial neural network
- Bayesian network
- Decision tree
- Parallel piped

After performing supervised classification, accuracy assessment is conducted to assess how well the classification process is achieved.

2.1.3.1 Accuracy assessment

Is an important for any classification project. It is used to compare the classified image to another data source or ground truth data. Accuracy assessment can be determined by an error matrix. An error matrix can be defined as the square array of numbers laid out in rows and columns that express the number of sample units assigned to a particular category relative to the actual category as verified in the field. Whereby the columns represent reference data, while the rows represent classification generated from remotely sensed data. The overall accuracy of the classification is determined by dividing the total correct pixels (sum of the major diagonal) by the total number of pixels in the error matrix (N) (Wang et al., 2012). According to Corine Land Cover Classification Scheme, more than 75% accuracy is valid.

Both supervised and unsupervised classification are pixel-based classification creating a square pixel-based classes.

3. Object-based image analysis

This technique is based on similar objects whereby pixels are categorized based on their spectral, shape, spatial relationship with the closest pixels, texture and, characteristics (Subha, 2019). Due to the improved research, spatial resolution of images is increased drastically (Wang et al., 2019). Hence research trend has oriented towards the object-based classification of images, classification based on pixel is gradually is becoming to no need. The trend is now becoming to more semantic processes reflecting human visualization.

The two most common segmentation algorithms are:

- Multi-resolution segmentation in eCognition
- The segment means shift tool in ArcGIS

Taking into consideration on multiresolution segmentation algorithm.

Multiresolution segmentation algorithm

A Multiresolution Segmentation (MRS) algorithm is frequently used in geomorphological studies; it minimizes the average intra-unit heterogeneity whereas maximizes the inter-unit heterogeneity of image objects by applying a mutual best-fitting approach (Sukeshini et al., 2020).

2.2.4 Classification schemes

The LCCS is a hierarchical a priori classification scheme built to provide a broad, yet flexible standardized classification system that would be effective at providing global scale land cover information (Di Gregorio, 2000).

2.2.5 Land use/ Landcover

The terms land use and land cover are often used interchangeably, but have a unique meaning. Land cover refers to the surface cover on the ground like vegetation, urban infrastructure, water, bare soil etc. And while land use refers to the purpose the land serves, for example, recreation, wildlife habitat, or agriculture (Satpalda, 2018). In general Land Use / Land Cover (LULC) refers to the categorization or classification of human activities and natural elements on the landscape within a specific time frame based on established scientific and statistical methods of analysis of appropriate source materials. Whereas LULC Classification is the process of appointing land cover classes to pixels and categorize them (Alshari & Gawali, 2021).

2.2.6 Change detection

Information about Land Use Land Cover Change (LULCC) is critical to improve our understanding of human interaction with the environment, and provide a scientific foundation for sustainability, vulnerability and resilience of land systems and their use (Wang et al., 2012).

Methods of change detection

- Image differencing
- Principal component analysis
- Post classification comparison
- Spectral mixture analysis
- Artificial neural networks
- Integration of geographical information system and remote sensing data (Lu et al., 2004).

2.2 DEM generation

DEM stands for Digital elevation model. It is a continuous variation of the Earth's topography, primarily stored within cells of a regular raster grid, and are the main input for a large variety of applications, including geomorphologic mapping of landforms (Braun, 2021). DEMs are created from different sources including conventional surveying techniques d as well as remote sensing techniques

DEM generation from InSAR is advantageous in remote areas where the photogrammetric approach to DEM generation is hindered by inclement weather conditions (Lu et al., 2012). Approaches used to generate DEM includes:

2.2.1 Ground survey techniques

By geolocating the horizontal and vertical position of points on the Earth's surface using theodolites with triangulation methods or by using GPS to create a dense mesh of observation points. Plotting these observations of location and elevation on paper or digitally in a computer software to create surface representation known as DEM.

Advantages of ground survey information.

- High accuracy.
- Flexibility.
- Require very little processing after the measurements have been taken.

Disadvantages of ground survey information.

- Equipments are expensive.
- Require intensive efforts.
- Time consuming.

2.2.2 From existing topographic maps

DEM can be obtained from existing topographic map by three ways:

- Manual digitizing of topographic maps.

The conversion of data presented in analogue form, such as maps and aerial photographs, into a digital form, is normally done manually by a human operator using a digitizer.

- The automated digitizing of cartographic maps

A semi-automated process for extracting features, using dedicated feature-recognition software to perform raster-to-vector conversion. The software automatically identifies the different thematic layers in the scanned image of the topographic map and splits them into separate raster layers. These layers are then edited manually to clean up the features and correct them, before they are converted into vectors, for further editing and labelling (Pike et al., 2009).

2.2.3 Remote sensing technique

Remote sensing technique used to generate DEMs are:

1. Photogrammetric land-surface models

Aerial photographs are essentially high-resolution, high-quality photographs taken from airborne platforms. By using survey data and Ground Control Points (GCP), these photographs can be geo-referenced, digitally. If several flight lines, or blocks of images for a geographic region with sufficient overlap typically 60% can be acquired, then stereo photos, and the stereo models associated with them, can be derived. To do this, ground control points and photogrammetric principles are used to extract the necessary elevation information (Pike et al., 2009).

2. InSAR.

InSAR stands for Interferometric Synthetic Aperture Radar. It is a remote sensing technique that can measure high resolution topographic profiles of the Earth's surface (Yu & Ge, 2010). Moreover, InSAR is a powerful tool in delineating Earth's topography and deformation (Massonnet et al., 1993). Interferometric approaches is used to detect surface deformations and as well as the derivation of digital elevation models (DEMs) (Braun, 2021).

An InSAR image, or interferogram, is produced by the combination of the phase components of two coregistered SAR images of the same area acquired from similar vantage points (Lu et al., 2012). InSAR digital elevation model (DEM) generation relies on the measurement of phase difference between the two sets of complex radar signals, i.e., the range difference between the satellite-borne radar instrument and the ground targets reflecting the radar transmissions.

General steps of generating DEMs using InSAR technique involves:

- Image coregistration.
- Formation of interferogram.
- Phase filtering.
- Multilooking.

- Phase unwrapping.
- Conversion of phase information into elevation.

2.3 Geomorphometry overview

Geomorphometry is defined as the quantitative measurement and analysis of the form of the earth's surface (Straumann, 2010). It can be best explained as a modern, analytical-cartographic approach to represent bare-earth topography by the computer manipulation of terrain height (Tobler, 2000). It based on science and practice of measuring the characteristics of terrain, the shape of the surface of the Earth, and the effects of this surface form on human and natural geography. While morphometry is a quantitative assessment of the geometry of a river basin and interpretation of the landforms in terms of their shape and size (Ali & Singh, 2022). Geomorphometry involves the use or without use of digital data which is more correctly considered a part of quantitative geomorphology (Thorn, 1988). According to Evans (1972), geomorphometric analysis can be addressed into two modes, which are specific (e.g., addressing discrete surface features such as landforms), and general which involves treating the continuous land surface.

Consider some of the basic terms which can be found in the study of geomorphometry:

- A land surface parameter is a descriptive measure of surface form (e.g., slope, aspect, wetness index). Normally it is arrayed in a continuous field of values, for the same referent area as its source DEM. It is also known as morphometric variables.
- A land-surface object is a discrete spatial feature (e.g., watershed line, cirque, alluvial fan, drainage network), best represented on a vector map consisting of points, lines, and/or polygons extracted from the square-grid DEM.

The main procedure taking place in the study of geomorphometry is the extraction of terrain parameters as well as objects. It takes place in five basic steps which are:

- Obtaining elevation data or measurements.
- Generating a surface model from the obtained data.
- Removing errors and artefacts from the generated surface model.
- Deriving land surface parameters and objects.
- Application of the resulting parameters and objects.

Recognition and delimitation of discrete features on a continuous surface is more difficult than that of elementary forms and thus Specific Geomorphometry remains the more subjective practice (Evans & Cox, 1974).

Application of geomorphometry:

- Environmental and Earth science applications such as monitoring landslides, depositional and erosional processes.

- Civil engineering and military applications.
- Applications in oceanography.
- Applications in planetary science and space exploration.
- Applications in the entertainment business.

Geomorphometry involve the extraction of land-surface parameters and objects from digital elevation models (DEMs).

2.3.1 Landforms

A landform is a physical feature of the Earth's surface that possesses a characteristic, recognizable shape and is produced by natural causes (Shary, 1995). Land surfaces consist of multiple landforms, each having different visual and physical characteristics. Different landforms differ to one another by either shape, size, orientation, relief and contextual position. Each landform may be composed of several landform elements, smaller divisions of the land surface that have relatively constant morphometric properties (Pike et al., 2009). Landforms can be classified into macro and micro landforms. Macro landforms are of four types that is mountains, hills, valleys and plains.

Landforms can be classified manually and automatically with the use of computer software.

Landforms are classified based on the physical characteristics such as elevation, slope, orientation, stratification, rock exposure, and soil type. Examples of those are hills, mountains, plateaus, canyons, valleys shoreline features such as bays, peninsulas, and seas, including submerged features such as mid-ocean ridges, volcanoes, and the great ocean basins (Sukeshini et al., 2020).

It is not possible to separate the mountain ranges from the basins and piedmonts by thresholds (Argialas & Miliaresis, 1997).

2.3.2 Landform classification and mapping

Automated extraction of specific landform elements from a DEM involves a more detailed level of abstraction and larger scale than classification of repeating landform types. The classification of landform elements involves segmentation of individual hillslopes into more or less homogeneous classes or facets along a catenary sequence such as from ridge crest to valley bottom following concepts outlined by Milne (1935) and elaborated by Ruhe and Walker (1968) and Huggett (1975). Taking examples Dikau (1989), Pennock et al. (1994), Fels and Matson (1996), Irvin et al. (1997), Zhu (1997), MacMillan et al. (2000), Etzelmüller and Sulebak (2000), Bui and Moran (2001), Burrough et al. (2001), Bathgate and Duram (2003) and Dr˘agu¸t and Blaschke (2006) (Pike et al., 2009). Taking example of characterization led by Wood (1996) and Dikau (1989)

Wood (1996) had 6 landforms classes which are peak (all neighbors lower), plain (no prominent curvatures defining distinct shapes), ridge (neighbors on two opposite sides lower), saddle

(neighbors on two opposite sides higher and on the orthogonal sides lower), channel (neighbors on two opposite sides higher) and pit (all neighbors higher).

Dikau (1989) had 9 landforms classes which are nose, spur, spur foot, shoulder slope, planar slope, foot slope, hollow shoulder, hollow and hollow foot

From the above researchers and many other previous researchers which came to provide characterization of landform classes several landform elements can be classified using several methods which include:

- Unsupervised classification
- Supervised classification.
- Object-based image analysis (OBIA).

CHAPTER THREE

METHODOLOGY

3.0 Introduction to methodology

This chapter provides the description of the location of the study area, description of datasets used, their specifications and as well as the site/source for which these datasets were collected. Additionally, the methods used to check the validity of the datasets and the methodological procedures adopted to reach the required output were also described in this chapter in a chronological manner. Flowcharts were used to facilitate easy understanding of the methodological procedures adopted.

3.1 Location of the study area

The Msimbazi basin is a part of Wami-Ruvu basin. It originates from Pugu hills flowing through the heart of Dar es salaam city and down washing to the coast to meet Indian ocean. The Msimbazi basin occupies about 15% of the total coverage of the Dar es salaam city thus having an area of about 350km^2. It is imaginary divided into three parts, the upper basin, the lower middle basin and the lower basin. The Msimbazi basin is geographically located between latitude -6,710^{o}S to -6.980^{o}S and longitude 38.29^{o}E to 39.29^{o}E having a highest altitude of about 312 m and lowest elevation of 5m. The climatic condition along the basin is humid tropical with a mean daily temperature along the basin varying between 18 ◦C and 33 ◦C. The Msimbazi basin experiences two seasons, wet and dry season. The wet season consist of two rainfall seasons which are high rainfall and low rainfall. The high rainfall is experienced in March–May with a monthly average of 150-300 mm of rainfall while the low rainfall is experienced in October–December with a monthly average range of 75-100 mm of rainfall while the annual average rainfall of about 1050mm. The main river found along the basin is known as Msimbazi river which is approximately 35km long. The economic activities that can be found along the basin include commercial, industrial and agricultural producing many vegetables and fruits that are supplied in Dar es Salaam city.

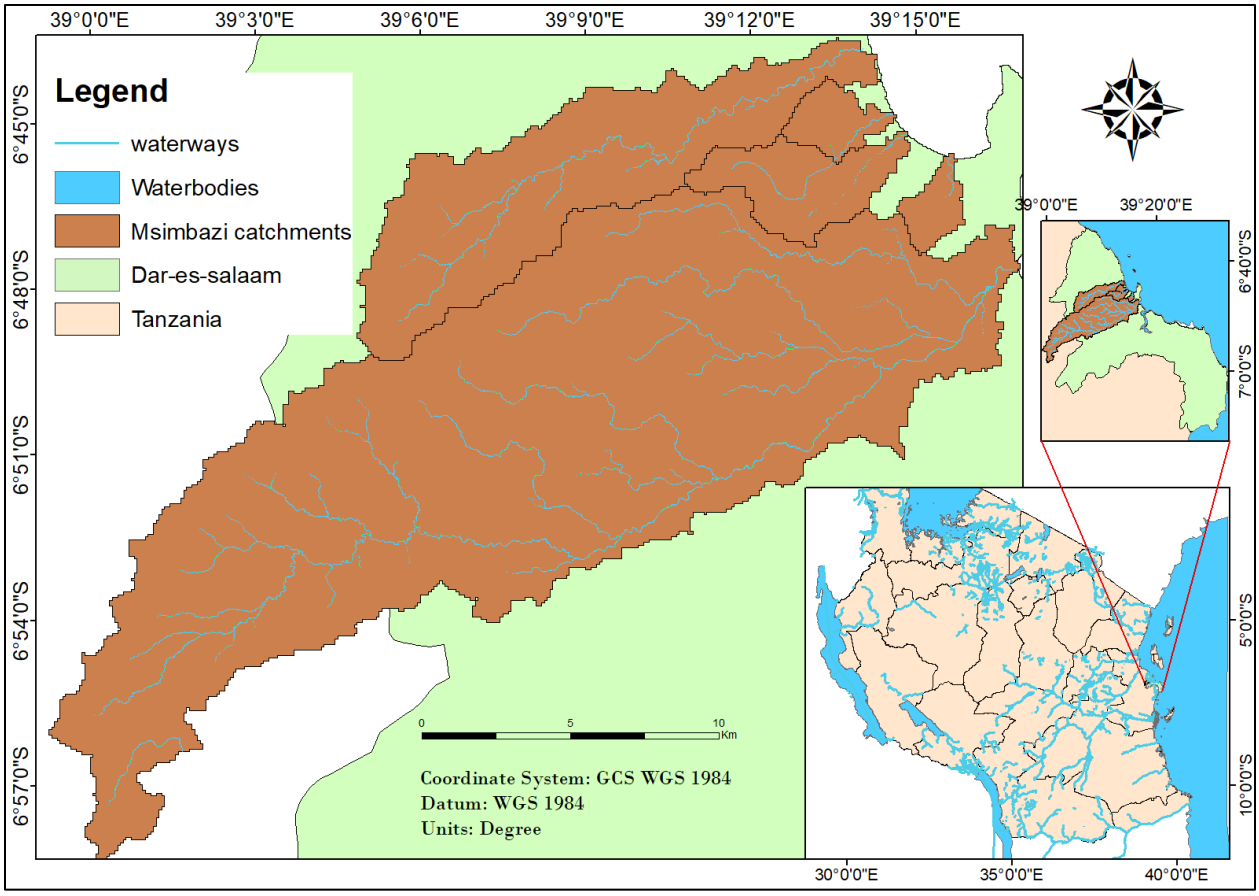

Figure 3-1: Location map of Msimbazi basin

3.2 Descriptions of the method and materials

The datasets used in this research included radar data, shapefile of the boundaries of the basin and optical dataset collected from different sources.

Table 3-1: Datasets used and their sources

s/n	Data	Spatial resolution	Time of acquisition	Source
1	Alos-1	12.5m ×12.5m	20/06/2009 & 05/08/2009	European Space Agency
2	Sentinel 1 SAR	10m × 10m	11/07/2022	https://scihub.copernicus.eu/apihub
3	SRTM DEM	30m ×30m	11/02/2000	USGS Earth Explorer
4	DTM	5m ×5m	01/12/2017	Tanzania Resiliency Academy

5	Msimbazi basin shapefile		23/10/2019	Resilience academy
6	Landsat 5 TM	30m ×30m	25/06/1995 & 01/07/2009	USGS Earth Explorer
7	Landsat 8 OLI	30m ×30m	03/06/2022	USGS Earth Explorer

The selection of the datasets was based on the availability of datasets to fit a purpose. For 1995 dataset used for the creation of LULC map was Landsat 5 TM since it was operating at that time. Conversely, due to the unavailability of DTM dataset and as well as two L band Radar dataset operating at that time which could be used to elucidate the terrain information in the same year, a DEM from SRTM acquired at 2000 from USGS was used instead to derive terrain parameters and create a landform map.

For 2009, the dataset used for classification was Landsat 5 TM and Alos-1 datasets. This is because the optical datasets had clouds and the radar datasets when used alone could not yield the required accuracy hence combination of ads from the optical and radar dataset was opted, in order to attain the valid accuracy of classification. The generation of DTM required two L-bands radar datasets acquired at slightly different positions hence the two Alos-1 data was used.

For 2022, the dataset used for classification was Landsat 8 OLI since it was operating at that time together with Sentinel 1 SAR. The same case as for year 2009. The DEM used was DTM obtained from Tanzania Resiliency Academy of 2017. The choice was due to the availability of data.

For this study a DTM is well suitable to serve the purpose since the terrain information is used to derive the purpose. However, inability to get DTM dataset for the year 1995 has led to the use of DEM which involve addition of DTM with tree canopy information and hence distortion in the information.

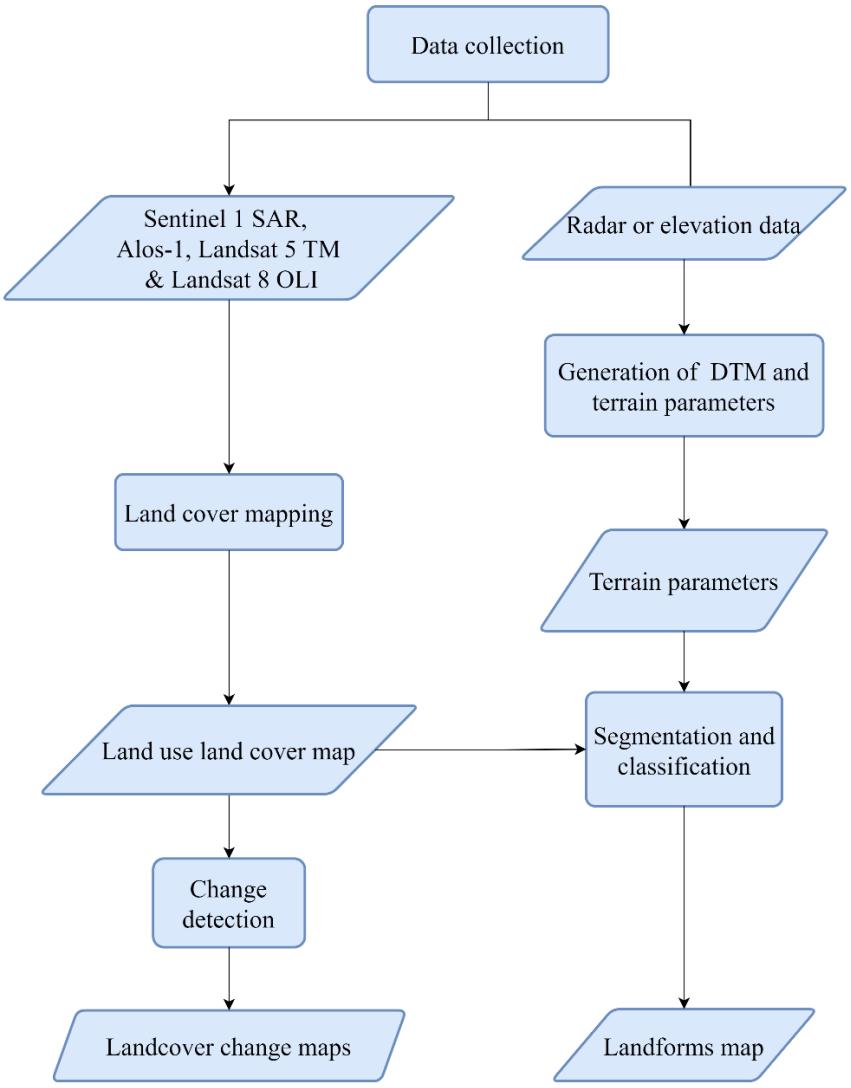

Figure 3-2: General methods used in generation of LULC maps, LULC change maps and landform maps

3.3 Land cover mapping and change detection

The procedure for landcover mapping followed systematic steps from the collection of the datasets till the retrieval of outputs. The obtained datasets for the formation of landcover maps were preprocessed and then classified in order to create LULC map and finally, a change in the landcovers was detected.

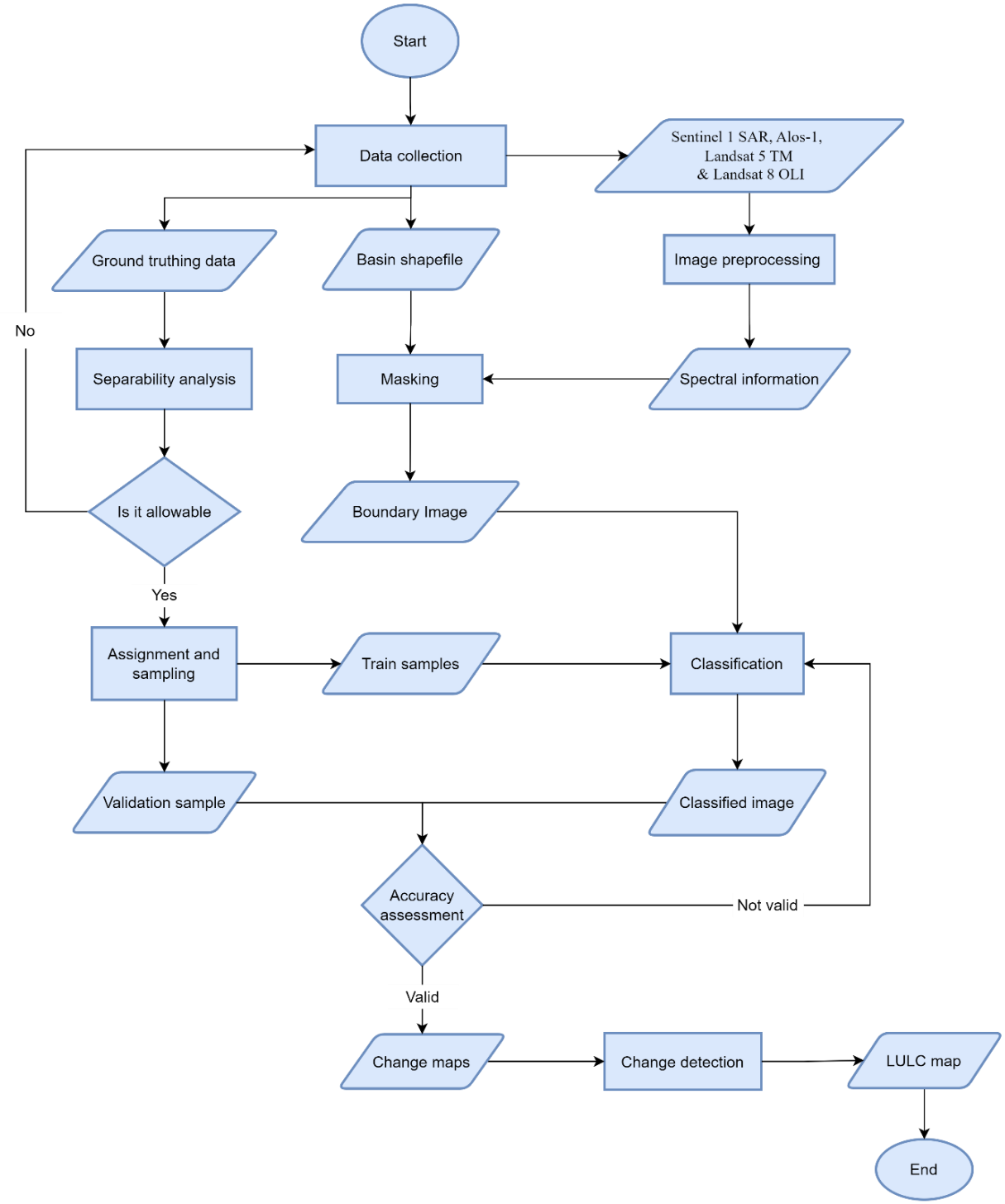

Figure 3-3: Workflow for landcover mapping and change detection

The classification technique used was unsupervised classification for 1995 while for 2009 and 2022 was supervised using random forest algorithm. The unsupervised classification was performed using Erdas Imagine software ad R studio was used to perform random forest

classification. The change detection method utilized here was post classification whereby a change in landcover was detected after performing landcover classification. To perform change detection, QGIS Desktop 3.30.2 software was used. Figure 3.2 shows the workflow followed at this stage.

3.3.1 Data collection

It involved the collection of remote sensing datasets, GIS data and ground truthing data.

- Ground truthing data

The ground truthing data collected were used for classification as well as for validation of the classification whereas 70% of the samples used was for classification ad 30% of the samples was used for validation. The data were obtained from google earth. Since google earth was launched in 2001, the sample data obtained were for the year 2009 and 2022. For the year 1995 since there was no means of obtaining the sample dataset and the area by that year was unfamiliar hence the method used for classification in 1995 was unsupervised classification. For the later years, the classification method opted was supervised classification. Based on previous researches conducted at the area and considering the aim of this research, the number of classes was 4 classes including water, barren land, urban or built-up land and vegetation using Anderson classification scheme. The distribution of the ground truthing data was diversified and covered the entire study area as seen from the figure below;

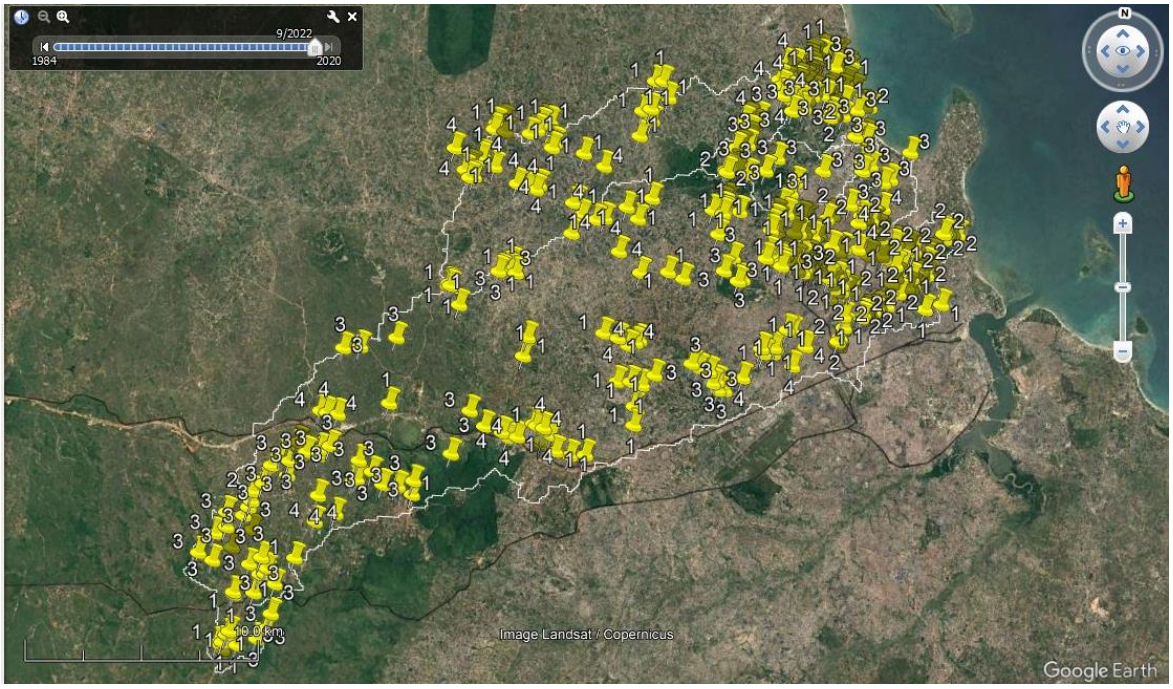

Figure 3-4: Example of ground truthing data distribution

- Remote sensing datasets

The imagery data obtained were from different site with different sensor. Two Landsat 5TM were collected for the year 1995 and 2009 and also Landsat 8 OLI data was collected for the year 2022. All these having a spatial resolution of 30m. In terms of SAR dataset, Jers-1 was collected for the year 1995, Alos-1 for the year 2009 and Setinel-1 for 2022 whereby the former had spatial resolutions of 12.5m and the later had a spatial resolution of 10m. All these datasets were collected from respective geoportal as shown in Table 3.1.

3.3.2 Checking the quality of ground truthing data

The quality check of the samples was well conducted by using separability analysis.

3.3.3 Preprocessing

- For the SAR datasets the preprocessing steps were as follows;

3.3.3.1 Radiometric Calibration

Using sentinel 1 toolbox, the first preprocessing method is to calibrate the SAR data before any other processing steps. All SAR datasets including Alos palsar dataset and the Sentinel-1 dataset were calibrated to provide the pixel values of an image be directly related to the scene radar backscatter. This process is essential to all level-1 SAR dataset hence, the radiometric calibration tool from Sentinel-1 toolbox was used to covert the level-1 SAR dataset into form of sigma nought values.

3.3.3.2 Multilooking

After calibration, multilooking was done to Alos-1 dataset only since it appeared to have non-squared pixel and the image quality was also poor. Multilooking aims to improve the image interpretability and visualization. Therefore, the radiometric calibrated Alos-1 data was converted from slant range to ground range by a process known as multilooking using Sentinel-1 toolbox to get squared pixels.

3.3.3.3 Subsetting

The data was large so the preprocessing steps, were delaying in time. To reduce bulkiness of the datasets, all of the datasets of all those three years were subset to a small area covering the area of interest one at a time.

3.3.3.4 Speckle filtering

The SAR datasets normally do have salt and pepper texturing effect. This effect reduces image interpretability and consequently misinformation. To reduce this effect the SAR datasets were speckle filtered using Single Product Speckle Filter after doing image subset. The resulting images appear to have less effect hence more interpretable. However, this step contradicts with the resolution of the image, the larger the widow size, the less the speckles, the lower the resolution

and vice versa. Therefore, a default 7 by 7 window was used in order not to counteract the resolution as well as removing some of the speckles.

3.3.3.5 Alos deskewing

For all Alos L1.1 datasets the annotated times are not zero Doppler like geometry meaning that the data is distributed in squinted geometry and hence influence the locational details Therefore, the Palsar dataset was deskewed after speckle filtering to adjust all the pixels to a more zero Doppler like geometry to account for geometric error.

3.3.3.6 Terrain correction

The geometric correction also involved terrain correction whereby the images were oriented to the original orientation of the area plus changing the projection into UTM with coordinate system of WGS84. The images were reprojected into projected coordinate system.

3.3.3.7 Linear to decibels

In order for the images to represent the actual spectral information from the ground, the images spectral information values were converted from linear to decibel using appropriate tool from Sentinel-1 toolbox.

3.3.3.8 Mosaicking

There were some datasets which required two scenes to cover the area of interest specifically the Sentinel-1 dataset. So, after all those preprocessing steps the images were mosaicked to cover the entire study area. Since all datasets were having two polarization bands in a sigma nought value, those bands were saved separately for the later use.

3.3.3.9 Resampling

The resulted output bands from the SAR datasets were up sampled to match with the other bands from optical imagery. The resulted bands had a spatial resolution of 10m. The resulted band from the year 2009 were HH and HV polarization bands and for 2022, they were VH and VV polarization bands.

- For the case of optical dataset Landsat images was used and preprocessed in QGIS software using SCP toolbox.

3.3.3.10 Radiometric correction

The radiometric preprocessing was done to the 4-band including Blue, Green, Red and NIR in QGIS platform. These 4 bands were for used for the classification processes because they have impact in detection of different land cover hence other bands were not considered. The SCP have tools for applying atmospheric correction for the images, all it requires is the input of the bands

and the MTL file (Landsat Metadata file). Additionally, the DN values were converted to spectral radiance in that process. The resulting datasets were radiometrically corrected.

3.3.3.11 Resampling

For the formation of landcover classes, the method involved the combination of different datasets from different sensors and consequently, the spatial resolution of the datasets also differs. In order to have a similar spatial resolution, the Landsat bands were resampled to meet the resolution of the corresponding SAR spatial resolution which was 10m.

3.3.3.12 Layer stack and reprojection

This process followed in order to combine those bands from the SAR dataset with the four bands from Landsat imagery to create a multispectral image consisting of six bands except for the year 1995 had 4 visible bands. Then the resulting image was reprojected into a projected coordinate system using WGS84/UTM 37S.

3.3.3.13 Clip

The multispectral image was covering more than the study area so the image was masked to the study area using the shapefile of the catchment area. The resulting image was ready for classification process. The image was saved in a tiff format for further steps.

3.3.4 Classification

For the year 2009 and 2022 the technique used for classification was a random forest classification done in R studio software. Considering the samples obtained from google earth, these samples were used for training the pixels bands as well as for validation. 70% of the samples were used for training the pixels and 30% of it were used to conduct accuracy assessment on the classified image result.

For the year 1995, the method used was unsupervised classification method and used the same four number of classes as from the former classification. By using K-means algorithm, a classified image was created for 1995.

3.3.5 Accuracy assessment

The classified images for the year 2009 and 2022 were then validated to assess how good the classification process was done. It was done in the same R studio software and the results were obtained. When the result of accuracy assessment has not reached the standard, the image was reclassified till the standard value is reached.

3.3.6 Change detection

The final land cover maps were later used to detect the changes occurred in the area over the years. The method used was post processing and the result was mapped. The process was done in a QGIS platform. The maps showing the change detection over the years were also created.

3.4 Generation of DTM

The method used for the generation of DTM is SAR interferometry using Snaphu unwrapping plugin in Sentinel-1 toolbox. The images used was Alos-1 image for the year 2009. For the year 1995 and 2022, DEM/DTM obtained from respective geoportals as shown in table 3.1. Hence there was need to generate for 2009 only. To obtain the elevation of the terrain for the study area, these datasets were selected due to the availability and since they utilize in the L-band. For the preparation of DTM, the SAR product type was SLC data with a sensor mode of IW. The preparation of DTM raster followed the following chronological steps as in figure below

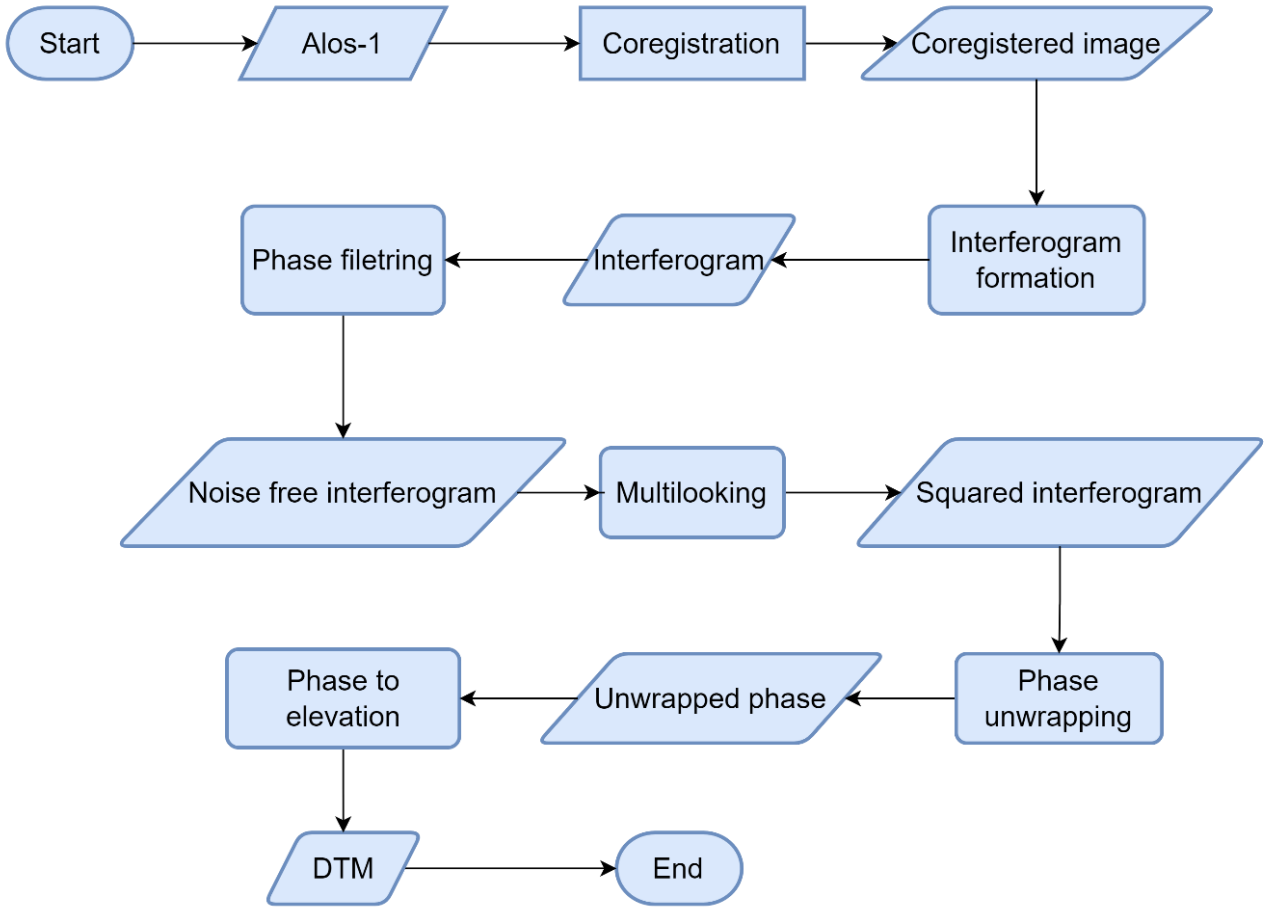

Figure 3-5: DTM generation workflow

3.4.1 Coregistration

To coregister images, the information about precise orbit and ephemeris is needed from the SAR sensor during acquisition. Therefore, applying the orbit file would be the first step before coregistration. But since the Alos datasets store these in the metadata file within the image file, therefore the application of orbit file become obsolete. Hence the first ever step is to coregister the two images into one coregistered image. These two images comprise images of the same year but taken at slightly different sensor position because it is necessary to have it taken at different position to obtain an interferogram. And the perpendicular baseline should be at least 150m apart. Using the coregistration tool from the toolbox, the images were coregistered as master and slave in a one image.

3.4.2 Formation of interferogram

To form the interferogram, the coregistered image was used as input in the interferogram tool. This tool provides an option of subtracting the topographic phase to get a deformation raster. But since the aim was the generation of DEM, that option was not opted. The result image is an interferogram with the phase band.

3.4.3 Phase filtering

To remove the noise present in the interferogram, the phase filtering was performed using Goldstein phase filtering tool to clear the noise in the interferogram. The resulted interferogram was clear from the noise and interpretable.

3.4.4 Multilooking

The azimuth and slant resolution of the interferogram was not equal. Therefore, to generate a squared pixel interferogram, multilooking was performed to the resulted interferogram using Multilook tool. With this step the dimension of the multilooked image is also reduced and hence make easy for unwrapping phase.

3.4.5 Phase unwrapping

Phase unwrapping in Sentinel-1 toolbox is performed using Snaphu export tool. Phase unwrapping occurs in three stages which are;

- Snaphu export

The phase band of the interferogram was exported and converted to a compatible snaphu format. The statistical cost-mode was made to be TOPO since the aim is to generate DEM.

- Snaphu unwrapping

Using the exported wrapped phase data of the interferogram and the Snaphu unwrapping tool, the phase data was now unwrapped into an image format.

- Snaphu import

Before importing the resulting image file, it was copied to the original dataset folder of the phase before unwrapping. Then by using Snaphu import tool, the unwrapped phase and the wrapped phase were used as an input in the process of importing the wrapped phase.

3.4.6 Conversion of phase into elevation

To create a DEM data, the unwrapped phase was used to convert it into elevation using the phase to elevation tool from the interferometric menu. The result is DEM specifically DTM and was exported into tiff format for further uses.

3.4.7 Resampling

The generated DTM plus the SRTM DEM and the obtained DTM were all resampled to a spatial resolution of 10m as the landcover maps.

3.5 Extraction of land surface parameter

Using the hydrological and surface modelling tools from ArcGIS platform, various landform derivatives were created, these were slope, aspect, hill shade, contour, flow accumulation, curvature (plan, profile and total), drainage network.

- Slope

A slope parameter was created using surface modelling tools and the measurement units of the raster was set to percent rise. The higher the percentage, the steeper the slope.

- Aspect

To display the direction of the slope, aspect raster was created to serve the purpose. This directly helps to understand the movement of the water across the area. To show the direction of the slopes 360^0 angle was used. The area which was flat was assigned a value of -1.

- Hillshade

To generate a hillshade raster, altitude and azimuth of the illumination source was needed. By using the default parameters from the toolbox, a hillshade was created.

- Flow accumulation

Before generation of the flow accumulation, flow direction raster is required to be generated first as it defines the direction of flowing water. Flow direction required only the DEM raster. For the

creation of flow accumulation, a material raster layer was created which was assigned a weight of one. This material raster was used together with the flow direction raster to give required output.

- Contours

Due to the nature of the area, the best option for the contour interval was 10m.

- Curvature

Profile, plan and total curvatures were created from the DEM dataset. The values of these curvatures were in terms of mm^{-1}.

- Drainage network

This is used to delineate the river or catchment. The first step involved was filling sinks as they would provide false information. The next step followed is to generate stream data by reclassifying the flow accumulation map to get the desired one which will be used to identify sinks. The value which perfectly fit our area is 500. Using the map algebra to export that stream data with the value. The next step was followed by creating stream links, it was followed by separating streams by stream order. Stream order identify streams based on their tributaries. Using Shreve method, a stream order was created. The last step was converting stream to feature.

3.6 Extraction of landforms

To extract the landforms, a multiresolution segmentation algorithm was opted to create morphometric regions. This process was followed by classifying the morphometric regions into appropriate landforms classes by using knowledge-based rules.

During classification of the morphometric regions to specific landforms, the 6 landforms from Wood (1996) and 9 landforms from Dikau (1989) was used combined and generate a total of 15 landform classes including peak (all neighbors lower), plain (no prominent curvatures defining distinct shapes), ridge (neighbors on two opposite sides lower), saddle (neighbors on two opposite sides higher and on the orthogonal sides lower), channel (neighbors on two opposite sides higher), pit (all neighbors higher), nose, spur, spur foot, shoulder slope, planar slope, foot slope, hollow shoulder, hollow and hollow foot.

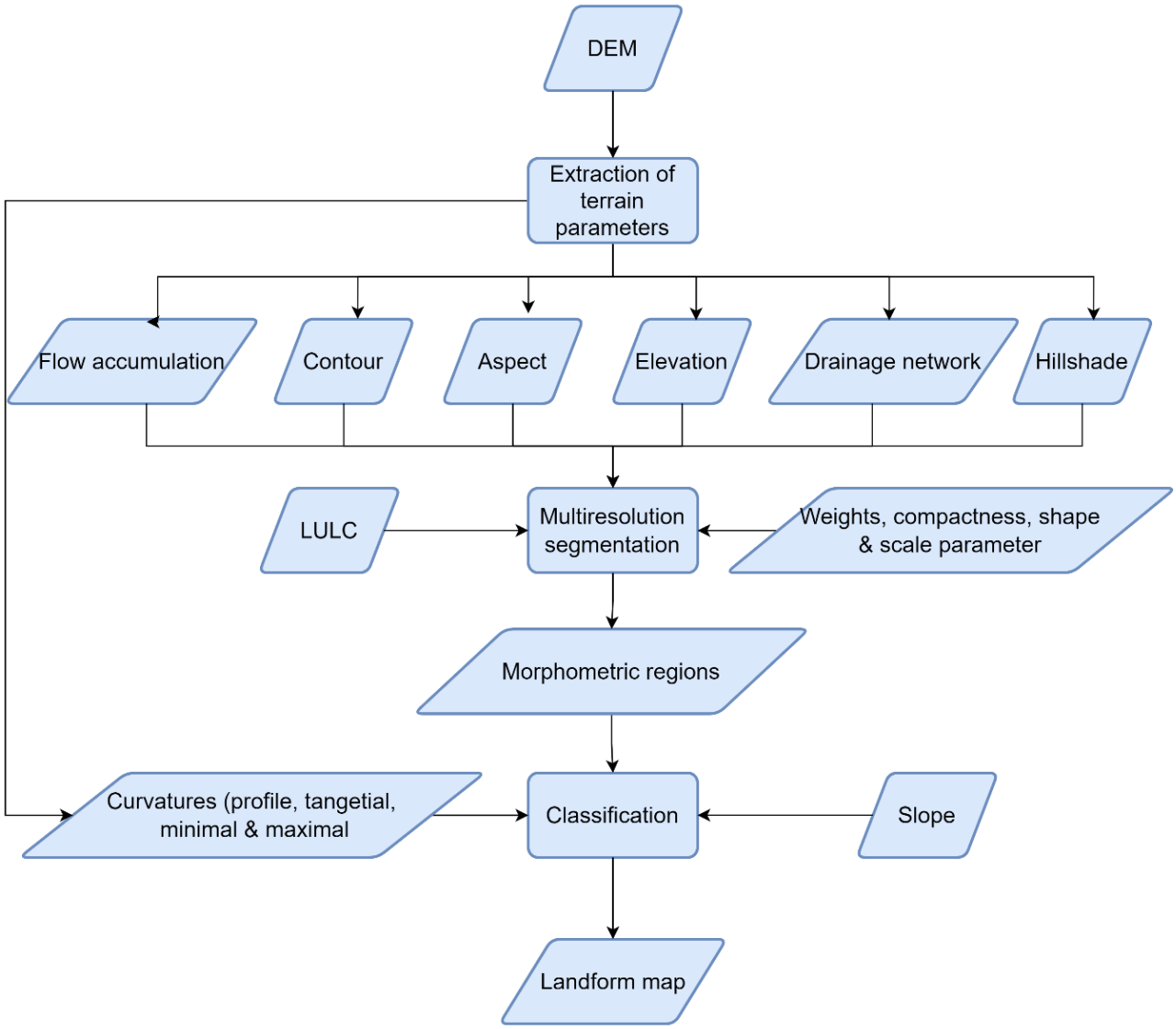

Figure 3-6: Extraction of landforms

3.7 Generation of landforms maps

After performing multiresolution segmentation algorithm, the map representing landforms was created and the change of the landforms was observed in a time series.

CHAPTER FOUR

RESULT, ANALYSIS AND DISCUSSION

4.0 Overview

This chapter highlights all the results obtained together with the analysis and discussion to the obtained output.

4.1 Classification results and land cover maps

The landcover maps created were having four classes including “Urban or built-up land”. “Water”, “Vegetation” ad “Barren land”. These four classes were chosen based o the aim of the analysis. The classification scheme used was Anderson classification scheme which provided the names for the classes. Due to the spatial resolution of the imagery, Anderson level 1 was used.

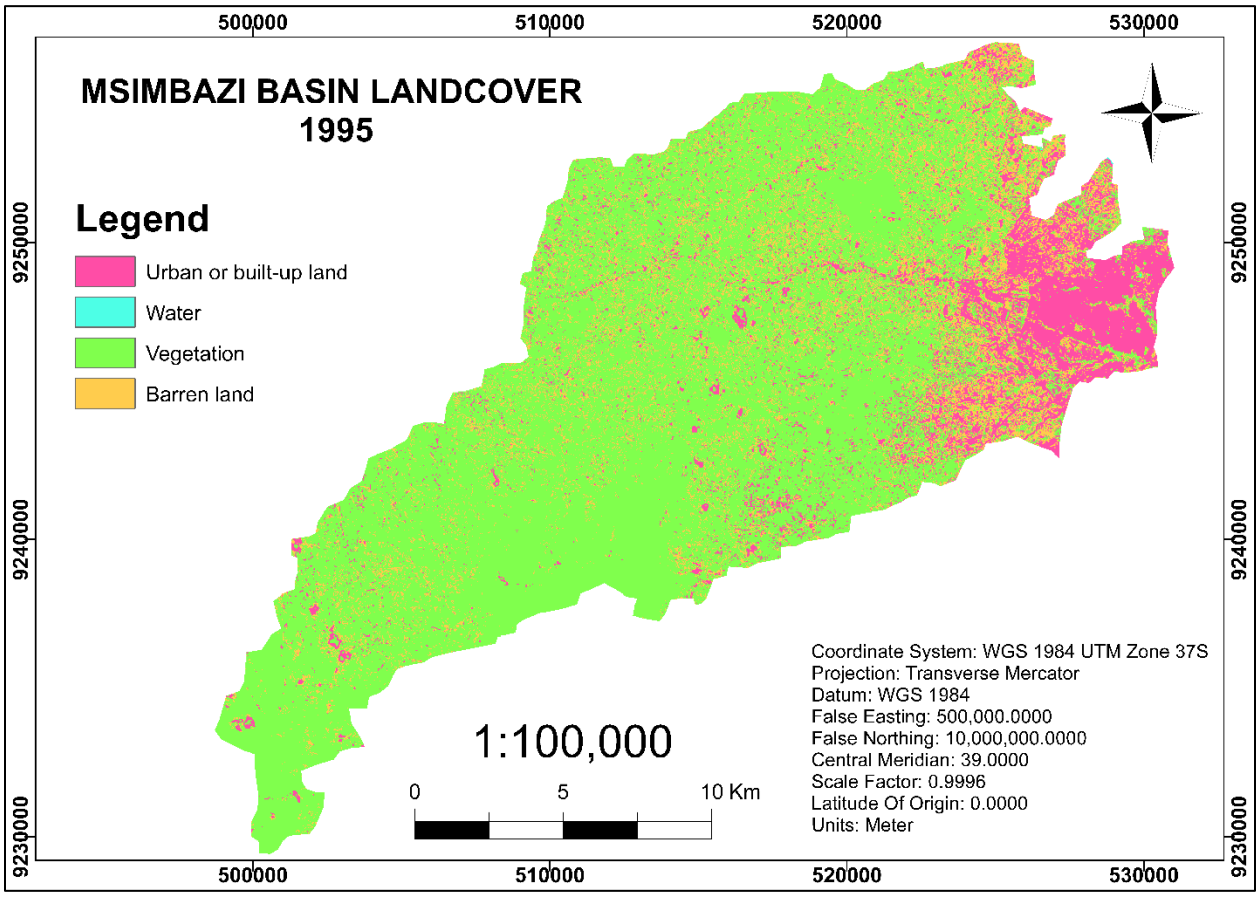

Figure 4-1: Msimbazi basin landcover map for the year 1995

In 1995 it can be seen from the fig 4.1 that large part of the area was covered by vegetation, whereas the built-up land was not large and was found at the south eastern side of the area.

Table 4-1: Percentages of land classes coverage in 1995

Landcover	Area (m^2)	Percentage (%)
Urban or built-up land	44131000	12.39%
Water	21700	0.01%
Vegetation	259607600	72.88%
Barren land	52439400	14.72%
Total	356199700	100.00%

About 72.88% of the entire area was covered by vegetation, 14.72% was covered by barren land, 12.39% was covered by urban area and 0.01% of the entire area was covered by water, consider table 4.1. At this time, the population at the basin was small but was concentrated at one part of the basin which implies even back at the days, the basin was still hazardous according to Dar es Salaam city master plan (Armstrong, 1987). The buildings were concentrated along the Msimbazi catchment.

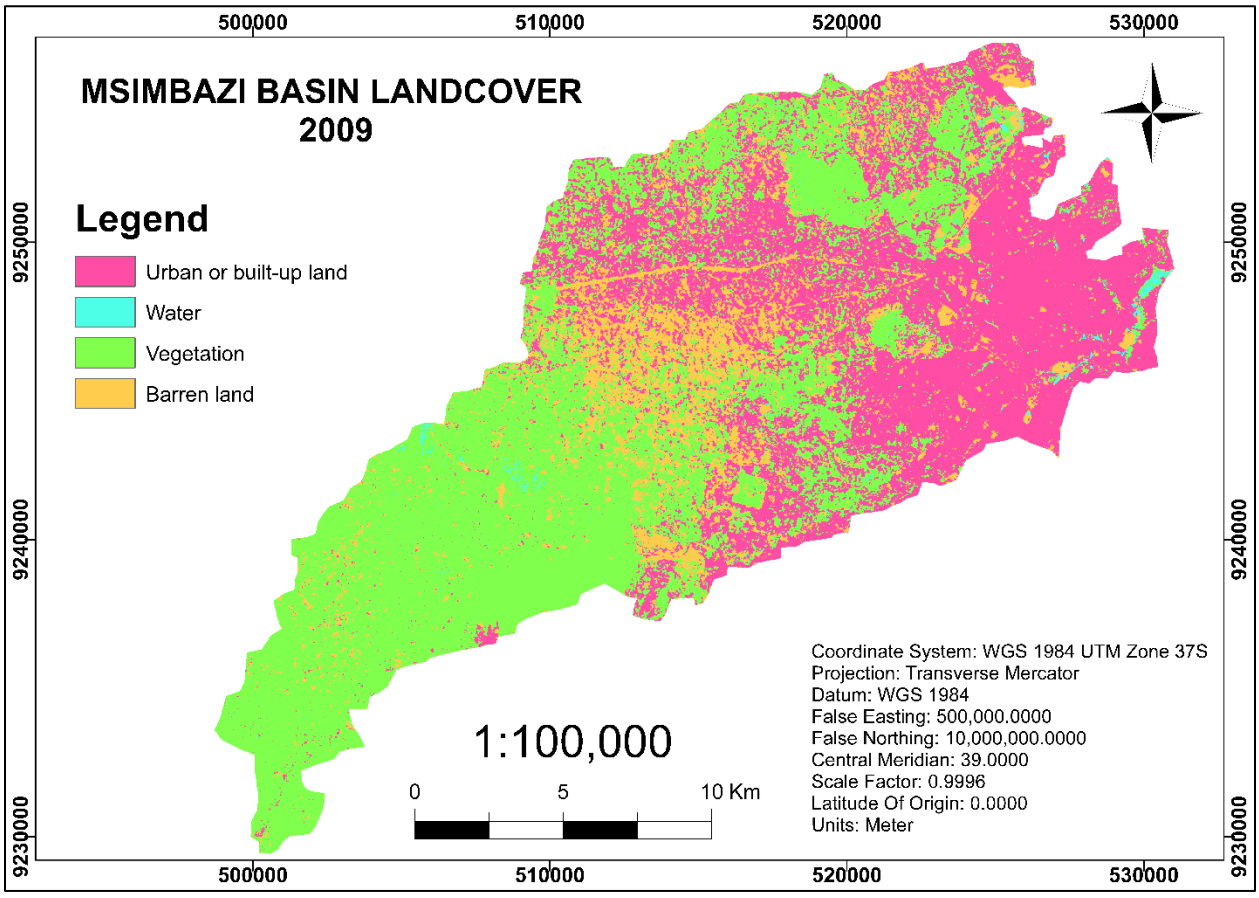

Figure 4-2: Msimbazi basin landcover map for the year 2009

In 2009, the vegetation was still large compared to other landcovers. Although vegetation still covers a large area when compared to other classes, it has decreased greatly when compared to 1995. Large part of vegetation was consumed by settlements as it can be seen in fig 4.2.

Table 4-2: Percentages of land classes coverage in 2009

Landcover	Area (m^2)	Percentage (%)
Urban or built-up land	136252500	38.22
Water	2841300	0.80
Vegetation	169564000	47.57
Barren land	47810800	13.41
Total	356468600	100.00

In 2009, "Vegetation" has covered about 47.57% of the total area, "Urban area" covered 38.22%, "Barren land" has covered about 13.41% of the entire basin and "Water" has covered 0.8% of the total basin. Water and urban area have increased while vegetation and barren land has decreased.

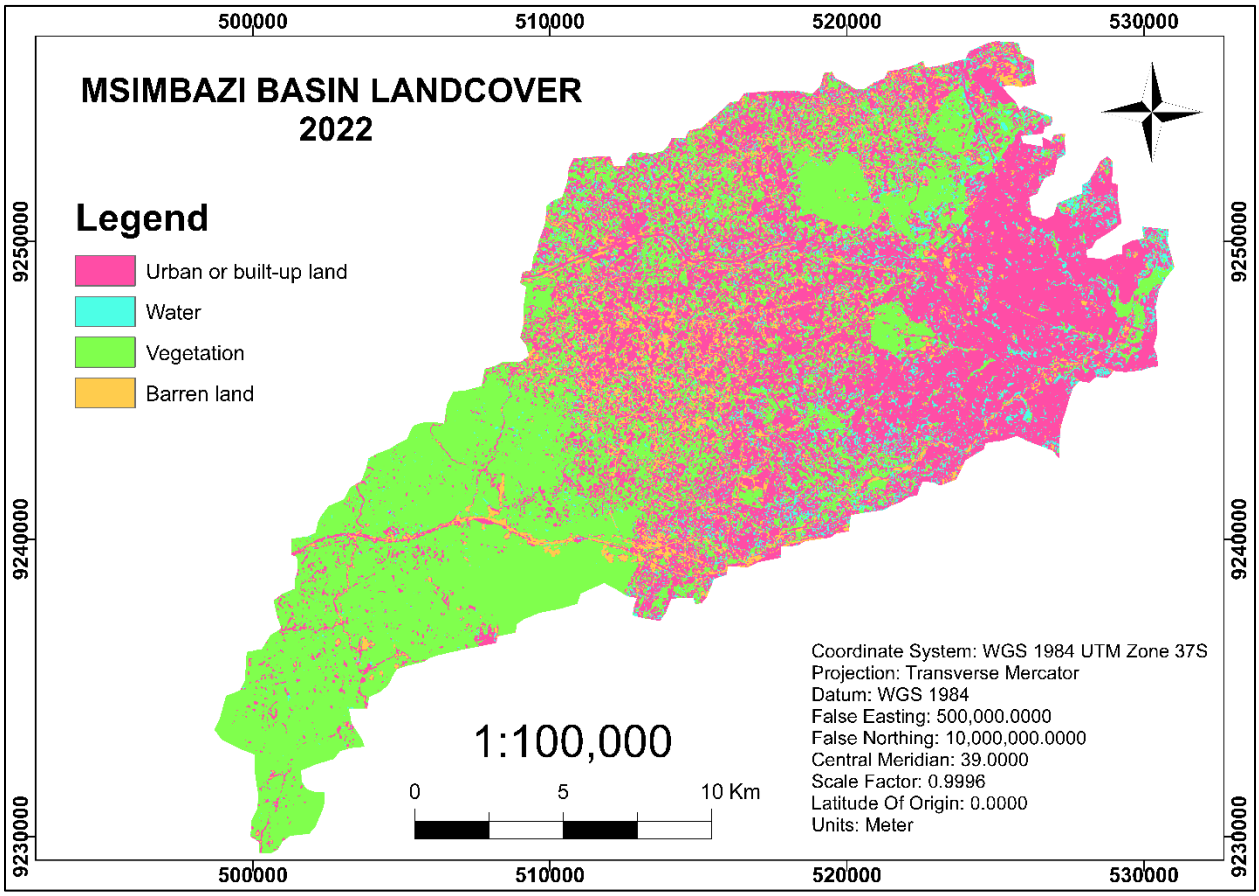

Figure 4-3: Msimbazi basin landcover map for the year 2022

It can be seen that the urban area now is more occupied at the basin compared to any other land class and more buildings have invaded the vegetation cover.

Table 4-3: Percentages of land classes coverage in 2022

Landcover	Area (m^2)	Percentage (%)
Urban or built-up land	155258200	43.55
Water	24941500	7
Vegetation	151120700	42.39
Barren land	25148200	7.05
Total	356468600	100

For about 43.55% of the total area is now occupied by urban area whereas vegetation occupies 42.39% of the area, barren land occupies 7.05% and water occupy 7% of the total area. The population around the basin is increasing to such an extent that it can be seen that the morphometry of the area is also changing through the increase of water class and decrease of vegetation. This is due to the fact that when a pervious surface is changed to an impervious surface, the ability of that surface to retain water decrease and therefore decrease of groundwater infiltration and increase surface water flow.

4.2 Accuracy assessment results

After performing classification, there was a need to check the reliability of the cover obtained. This process is known as accuracy assessment, it helps to show if the obtained cover has met the standard of classification. Below are the accuracy assessment reports obtained for 2009 and 2022.

Table 4-4: Confusion Matrix and Statistics for the Accuracy Assessment for the year 2009

		Producer						
User		Urban or built-up land	Water	Vegetation	Barren land	Total	Error of omission	Producer accuracy
	Urban or built-up land	49	2	4	4	59	16.95%	83.05%
	Water	0	6	0	0	6	0.00%	100.00%
	Vegetation	5	1	26	2	34	23.53%	76.47%
	Barren land	4	0	0	7	11	36.36%	63.64%
	Total	58	9	30	13	110		
	Error of commission	15.52%	33.33%	13.33%	46.15%			

	User accuracy	84.48%	66.67%	86.67%	53.85%			
Overall Statistics								
Accuracy	0.8							
95% CI	(0.713, 0.8702)							
No Information Rate	0.5273							
Kappa	0.6756							

The overall accuracy of classification for 2009 was 80% which was valid according to Anderson. Whereby the producer's accuracy for Urban or built-up land was 83.05%, for water was 100%, for vegetation was 76.47% and for barren land was 63.64%. For barren land the producer's accuracy was low because some pixels were confused with the class of built-up land due to some buildings appeared to have the same spectral color as the barren land.

Table 4-5: Confusion Matrix and Statistics for Accuracy assessment for the year 2022

	Producer							
User		Urban or built-up land	Water	Vegetation	Barren land	Total	Error of omission	Producer accuracy
	Urban or built-up land	45	3	1	2	51	11.76%	88.24%
	Water	7	17	2	1	27	37.04%	62.96%
	Vegetation	0	2	29	1	32	9.38%	90.63%
	Barren land	5	1	0	12	18	33.33%	66.67%
	Total	57	23	32	16	128		
	Error of commission	21.05%	26.09%	9.38%	25.00%			
	User accuracy	78.95%	73.91%	90.63%	75.00%			
Overall Statistics								
Accuracy	0.8047							
95% CI	(0.7253,0.8694)							
No Information Rate	0.4453							
Kappa	0.7228							

The accuracy assessment yield for year 2022 was valid with an overall accuracy of 80.47%. The producer's accuracy for urban or built-up land was 88.24%, for water was 62.96%, for vegetation was 90.63% and for barren land was 66.67%. The producer's accuracy for water was low because some of the pixels were classified as vegetation due to the vicinity existing between these two classes. You may find an area where there is a present of water, vegetation was also present. For barren land, the reason is the same as for 2009.

Since the classified images were valid, they were used to a letter stages.

4.3 Change detection results and analysis of the change for 1995 to 2009 and 2009 to 2022

After performing classification, a change was detected in the distribution of the landcovers from 1995 to 2022. To detect and quantify these changes of the landcovers, change detection was done to see a change on a series of landcover maps.

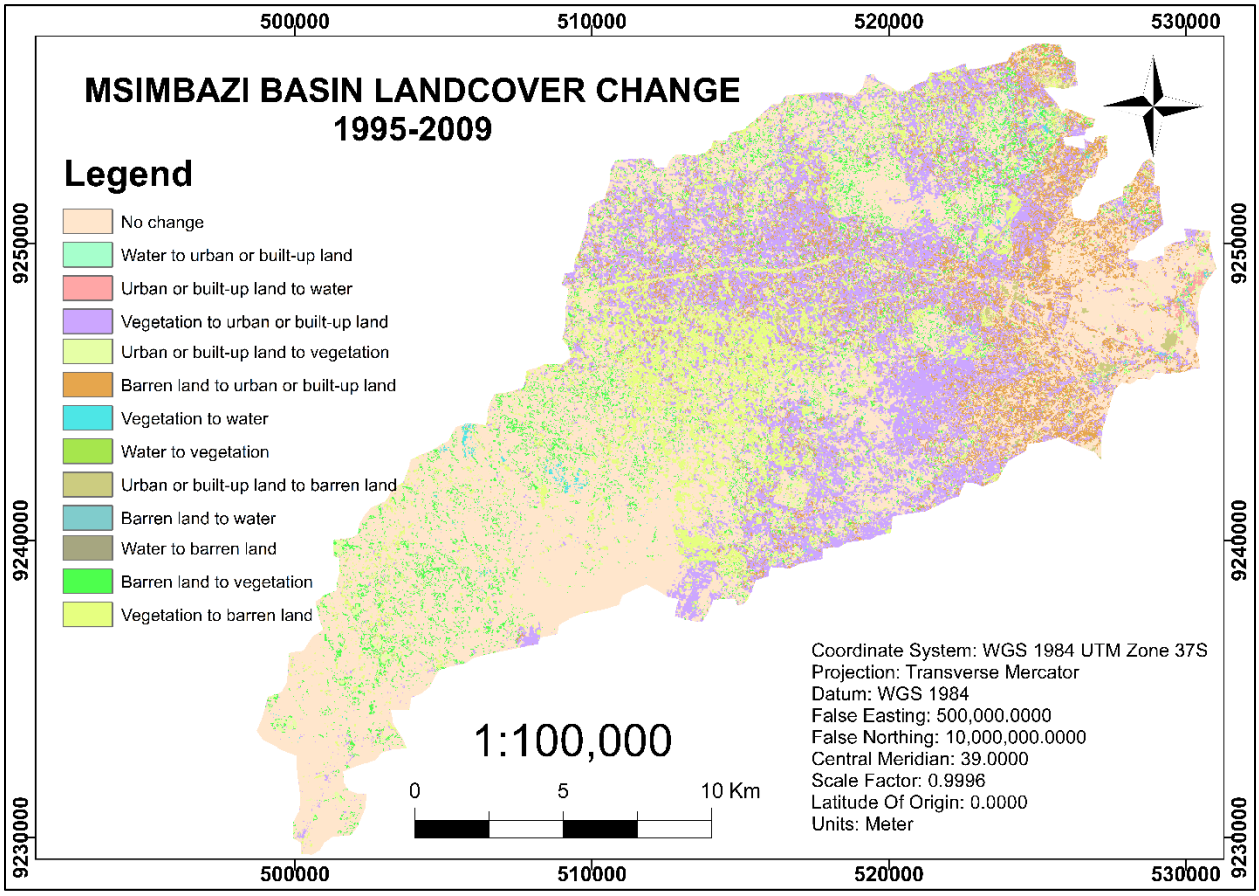

Figure 4-4: Msimbazi basin landcover change map from 1995 to 2009

From 1995 to 2009, a large portion of the overall area have not changed to another class although there was transition from one class to another. At most this transition was found from vegetation whereby mostly vegetation changed to urban area. The transition was also seen from vegetation to

barren land, barren land to urban, barren land to vegetation as well as considerable small other transitions as seen in fig 4.4.

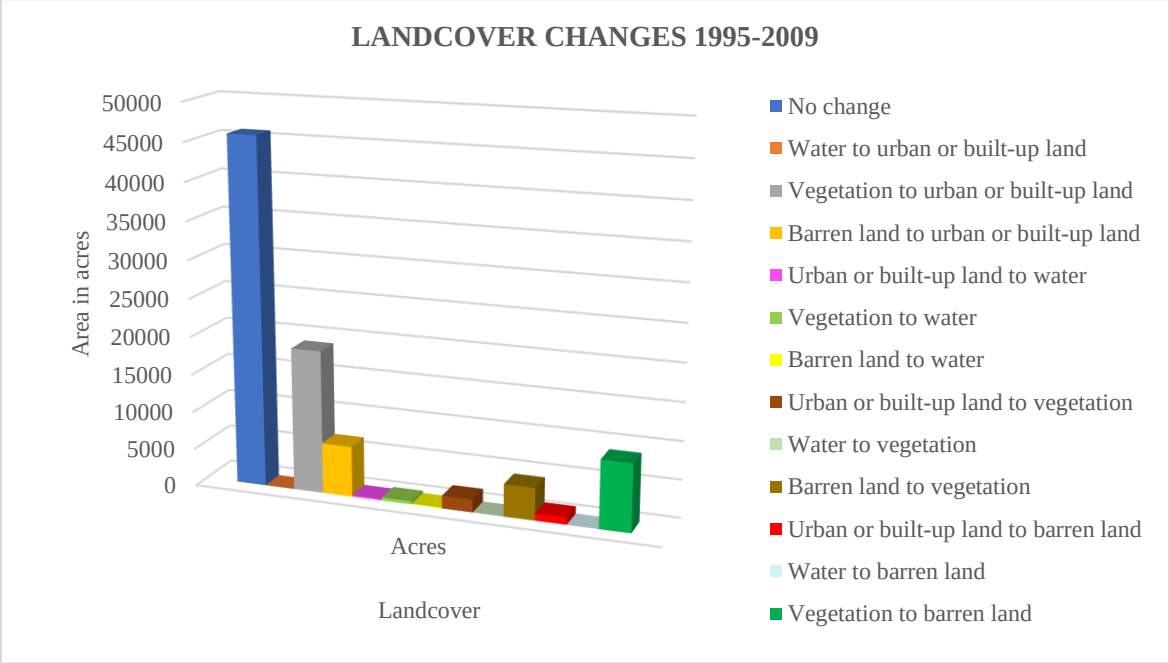

Figure 4-5: Graph showing landcover change from 1995 to 2009

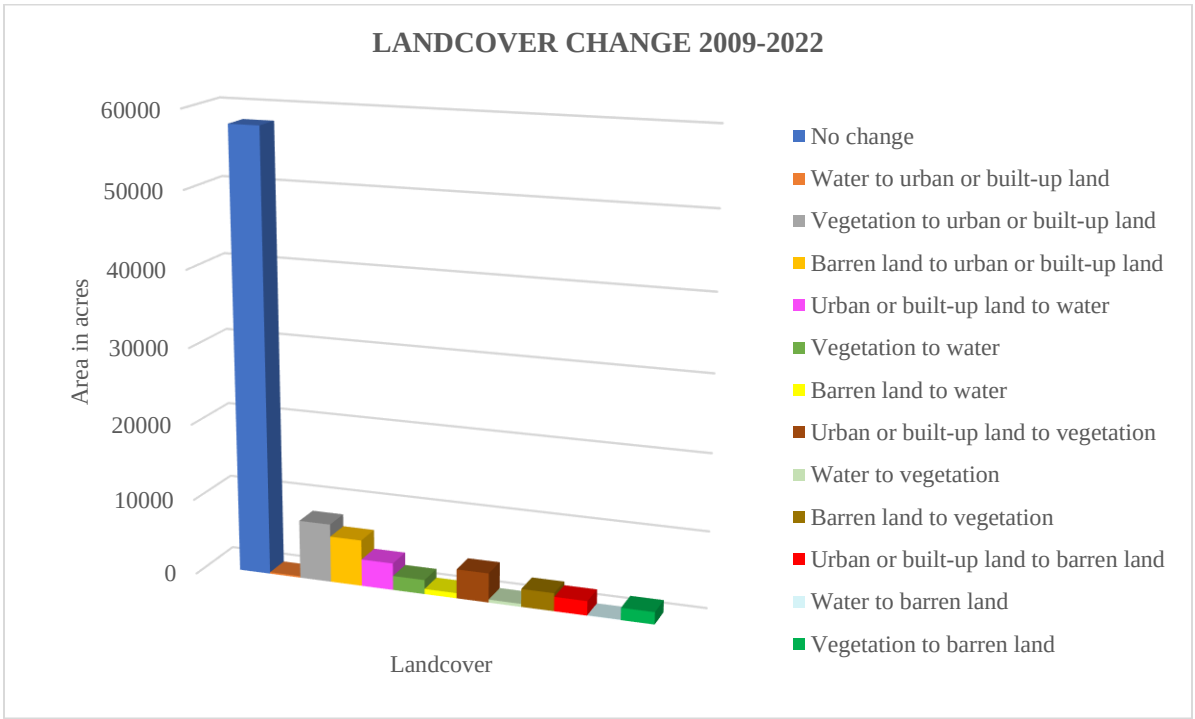

Figure 4-6: Graph showing landcover change from 2009 to 2022

From 2009 to 2022, large portion did also not change, basically a large part of the area covered by vegetation and urban area did not change as see in fig 4.7. There was also major transition from one class to another but the change was not large.

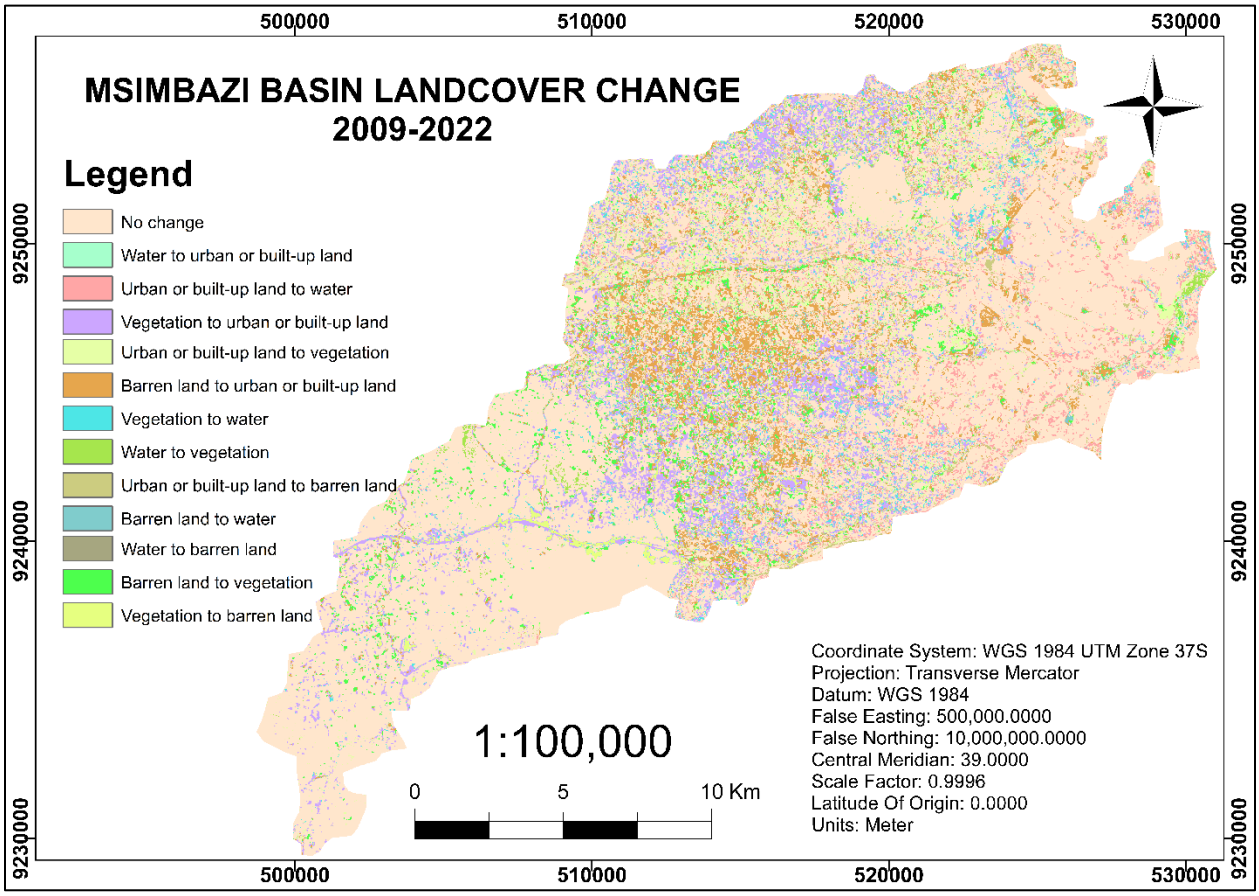

Figure 4-7: Msimbazi basin landcover change map from 2009 to 2022

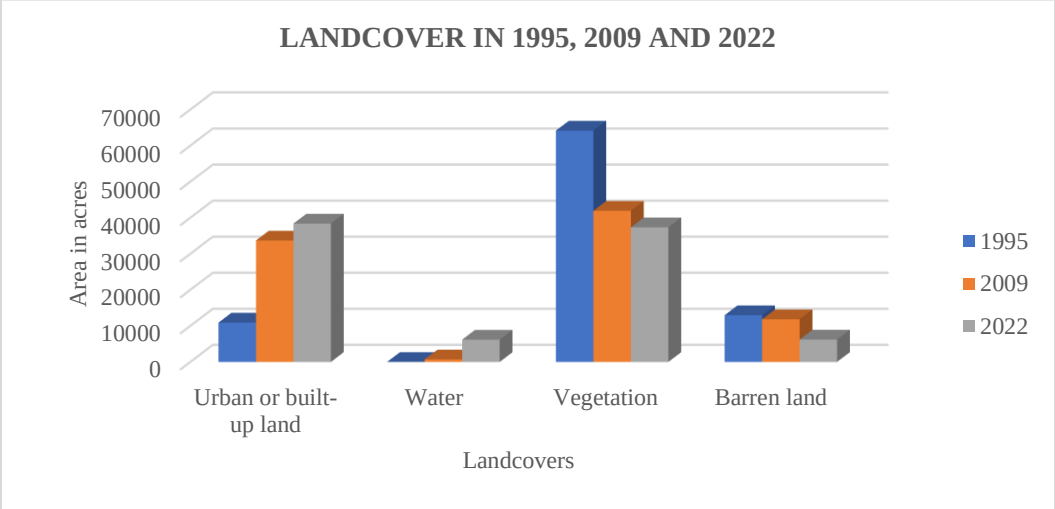

Figure 4-8: Graph showing landcover change from 1995 to 2022

4.4 Landform classification results and maps

Classification of the landforms was based on the classification criteria of landforms created by Wood (1996) and Dikau (1989). Thus, a total of 15 landforms were generated for the basin.

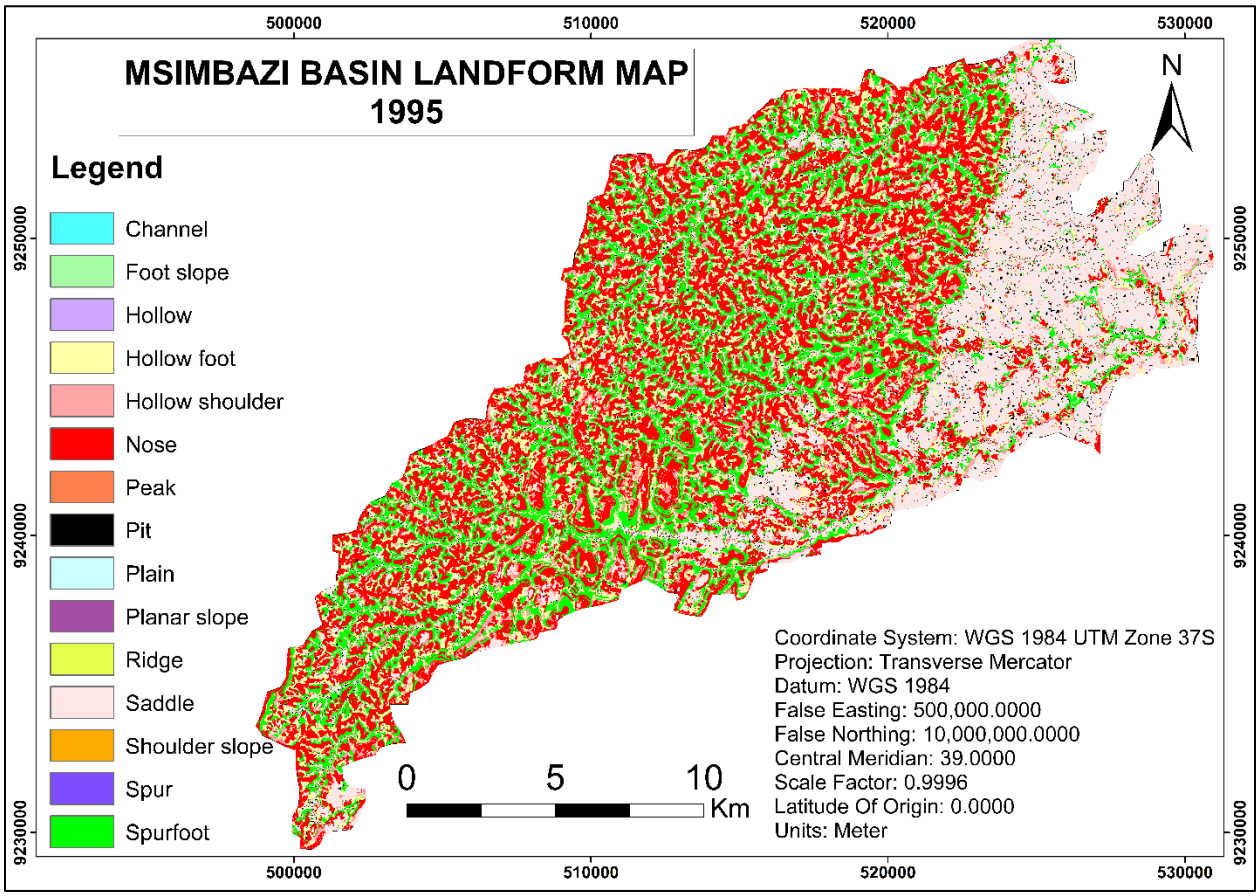

Figure4-9: Msimbazi basin landform map for the year 1995

For the year 1995 the landform classes which were preset at particular time were peak, plain, ridge, saddle, channel, pit, nose, spur, spur foot, shoulder slope, planar slope, foot slope, hollow shoulder, hollow and hollow foot. Whereby a large portion of the basin was a nose, followed by a saddle. Saddle is seen to occupy the lower portion of the basin (northeast of the basin/ near basin mouth area) whereby few other landform classes were also found to be dispersed along the area. These other landforms were mostly peaks, plains, pit, nose, spur foot and hollow shoulder. While at the upper basin area was largely covered by nose.

Table 4-6: Area coverage and percentage of landforms coverage in 1995

S/N	Landform type	Area (m^2)	Percentage (%)
1	Channel	457300	0.128
2	Foot slope	780500	0.219

3	Hollow	216900	0.061
4	Hollow foot	51669100	14.485
5	Hollow shoulder	19783900	5.546
6	Nose	119363200	33.463
7	Peak	1615300	0.453
8	Pit	8357700	2.343
9	Plain	6550800	1.836
10	Planar slope	256100	0.072
11	Ridge	106200	0.030
12	Saddle	80333400	22.521
13	Shoulder slope	86900	0.024
14	Spur	40100	0.011
15	Spur foot	67087000	18.807

For the year 1995, the percentage coverage of channel was 0.128%, foot slope was 0.219%, hollow was 0.061%, hollow foot was 14.485%, hollow shoulder was 5.546%, nose was 33.463%, peak was 0.453%, pit was 2.343%, plain was 1.836%, planar slope was 0.072%, ridge was 0.030%, saddle was 22.521%, shoulder slope was 0.024%, spur was 0.011% and spur foot was 18.807%.

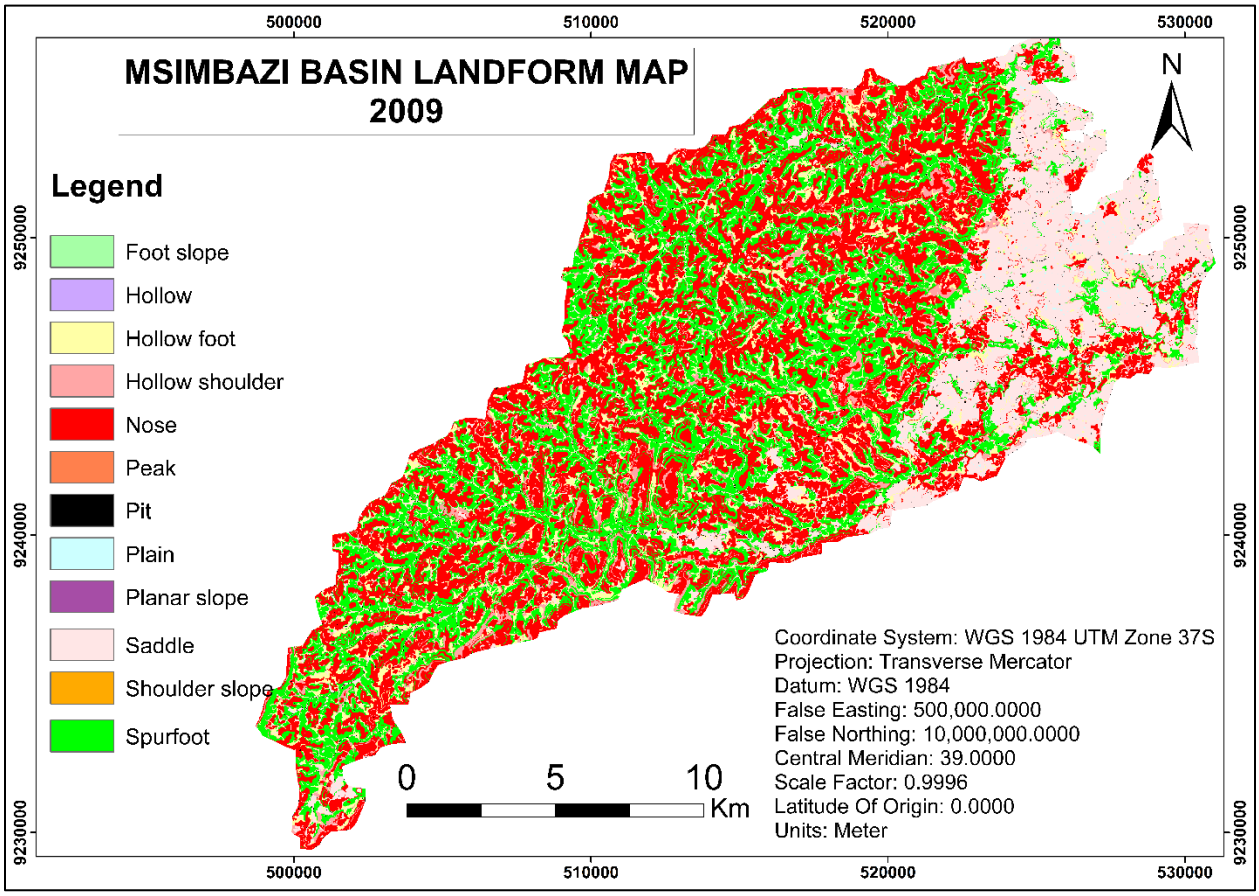

Figure 4-10: Msimbazi basin landform map for the year 2009

For 2009, the landforms present were peak, plain, saddle, pit, nose, spur foot, shoulder slope, planar slope, foot slope, hollow shoulder, hollow and hollow foot. Whereby, ridge, channel and spur were not preset at the area. Saddle and nose occupied the basin similarly as for 1995 but it can be seen that the dispersion of other landforms at the area covered mostly by saddle was small compared to 1995.

Table 4-7: Area coverage and percentage of landforms coverage in 1995

S/N	Landform type	Area (m^2)	Percentage (%)
1	Channel	0	0.000
2	Foot slope	5300	0.001
3	Hollow	500	0.000
4	Hollow foot	35365500	9.915
5	Hollow shoulder	16207800	4.544
6	Nose	136481800	38.262
7	Peak	370400	0.104
8	Pit	2333800	0.654
9	Plain	823300	0.231
10	Planar slope	18500	0.005
11	Ridge	0	0.000
12	Saddle	66479400	18.637
13	Shoulder slope	3400	0.001
14	Spur	0	0.000
15	Spur foot	98614700	27.646

For the year 2009, the percentage coverage of channel was 0.000%, foot slope was 0.001%, hollow was 0.000%, hollow foot was 9.915%, hollow shoulder was 4.544%, nose was 38.262%, peak 0.104%, was pit was 0.654%, plain was 0.231%, planar slope was 0.005%, ridge was 0.000%, saddle was 18.637%, shoulder slope was 0.001%, spur was 0.000% and spur foot was 27.646%.

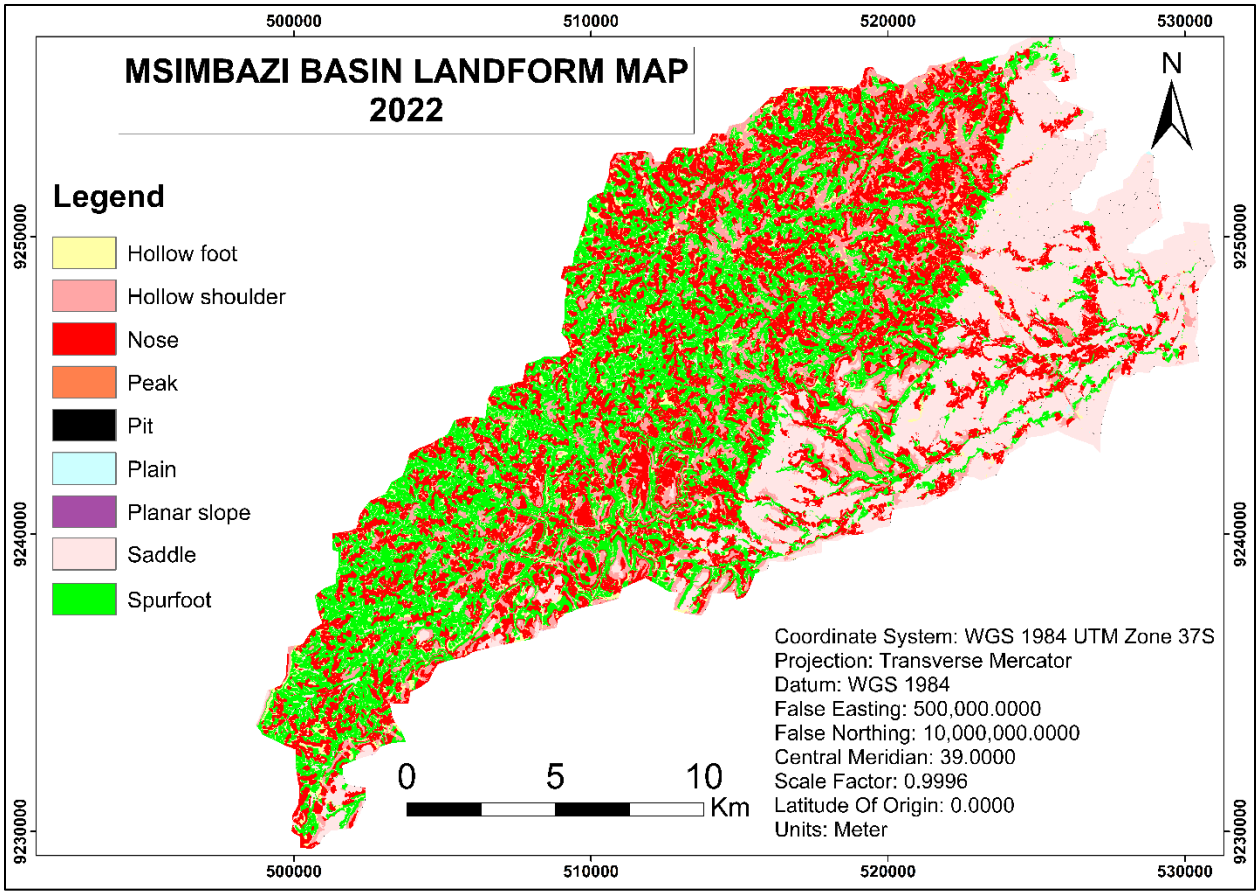

Figure 4-11: Msimbazi basin landform map for the year 2022

For 2022, the landforms preset were peak, plain, saddle, pit, nose, spur foot, planar slope, hollow shoulder, and hollow foot. Whereby channel, foot slope, hollow, ridge, shoulder slope and spur were not present at this time. This shows a huge difference to 1995 but the distribution of nose and saddle was the same as 1995 and 2009. However, the saddle the northeast region contained a little landform along the saddle.

Table 4-8: Area coverage and percentage of landforms coverage in 1995

S/N	Landform type	Area (m^2)	Percentage (%)
1	Channel	0	0.000
2	Foot slope	0	0.000
3	Hollow	0	0.000
4	Hollow foot	21109600	5.918
5	Hollow shoulder	33425900	9.371
6	Nose	110716600	31.039
7	Peak	15800	0.004
8	Pit	398300	0.112

9	Plain	89200	0.025
10	Planar slope	3500	0.001
11	Ridge	0	0.000
12	Saddle	83754600	23.480
13	Shoulder slope	0	0.000
14	Spur	0	0.000
15	Spur foot	107190900	30.050

For the year 2022, the percentage coverage of channel was 0.000%, foot slope was 0.000%, hollow was 0.000%, hollow foot was 5.918%, hollow shoulder was 9.371%, nose was 31.039%, peak was 0.004%, pit was 0.112%, plain was 0.025%, planar slope was 0.001%, ridge was 0.000%, saddle was 23.480%, shoulder slope was 0.000%, spur was 0.000% and spur foot was 30.050%.

4.5 Trend in the change of landform

The change can be seen in the Northeast of the basin whereby it changed from a terrain with variable landforms to a terrain occupied by a single landform which is saddle landform. Whereby the change was seen to systematically decrease along the series of time from 1995 to 2022.

Table 4-9: A change in the number of landforms with respect to area covered by built-up land

Year	Area covered by built-up land	Number of landforms
1995	44131000	15
2009	136252500	12
2022	155258200	9

Also, with the increase of area covered by Urban or built-up land, there seems to be a decrease to the number of basin landforms. Such that in 1995 the number of basin landforms was 15 while in 2009 was 12 and consequently 2022 was 9 landforms with the increase of area covered by built-up land systematically.

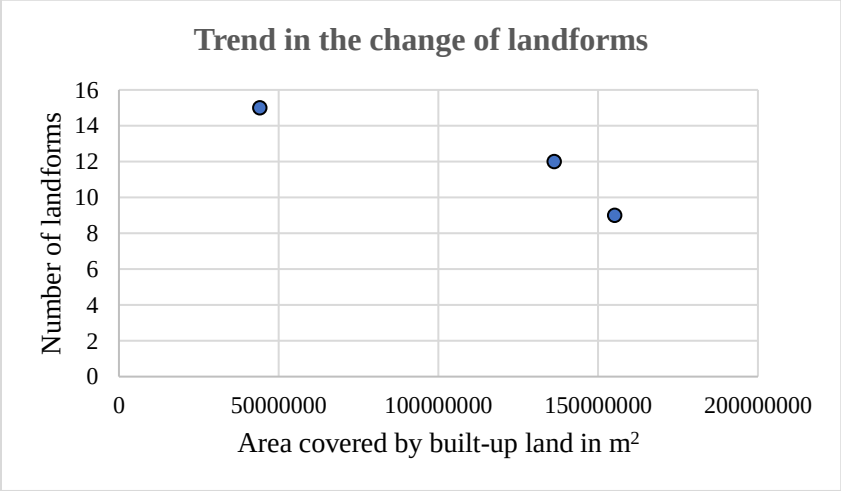

Figure 4-12: Trend of landform change with respect to area covered by Urban or built-up land

CHAPTER FIVE

CONCLUSION AND RECOMMENDATION

5.1 Conclusion

From the obtained classification results, the percentage of each landcover is as follows:

- In 1995, about 72.88% of the entire area was covered by vegetation, 14.72% was covered by barren land, 12.39% was covered by urban area and 0.01% of the entire area was covered by water.
- In 2009, vegetation covered about 47.57% of the total area, urban area covered 38.22%, barren land covered about 13.41% of the entire basin and water covered 0.8% of the total basin.
- In 2022, about 43.55% of the total area is now occupied by urban area whereas vegetation occupies 42.39% of the area, barren land occupies 7.05% and water occupy 7% of the total area

All these depicts that the built-up land increasing considerably from 1995 to 2009.

From the obtained landform map, the percentage of each landform is as follows:

- In 1995, the percentage coverage of channel was 0.128%, foot slope was 0.219%, hollow was 0.061%, hollow foot was 14.485%, hollow shoulder was 5.546%, nose was 33.463%, peak was 0.453%, pit was 2.343%, plain was 1.836%, planar slope was 0.072%, ridge was 0.030%, saddle was 22.521%, shoulder slope was 0.024%, spur was 0.011% and spur foot was 18.807%.
- In 2009, the percentage coverage of channel was 0.000%, foot slope was 0.001%, hollow was 0.000%, hollow foot was 9.915%, hollow shoulder was 4.544%, nose was 38.262%, peak 0.104%, was pit was 0.654%, plain was 0.231%, planar slope was 0.005%, ridge was 0.000%, saddle was 18.637%, shoulder slope was 0.001%, spur was 0.000% and spur foot was 27.646%.
- In 2022, the percentage coverage of channel was 0.000%, foot slope was 0.000%, hollow was 0.000%, hollow foot was 5.918%, hollow shoulder was 9.371%, nose was 31.039%, peak was 0.004%, pit was 0.112%, plain was 0.025%, planar slope was 0.001%, ridge was 0.000%, saddle was 23.480%, shoulder slope was 0.000%, spur was 0.000% and spur foot was 30.050%.

From the obtained result, it can be concluded that the morphometry of the basin changed in terms of the landforms covering the basin. With the increase of population around the basin. The change was seen only at the part where there was settlement. In areas around Pugu hills and other areas where there was no settlement, the morphometry was still the same. Hence population plays an important role in the morphometric changes of the basin. Such as

- From 1995 to 2009, at the lower reaches of the basin, it was noted some of the pits were filled in 2009.
- Also, from 2009 to 2022, all pits were completely filled leaving the lower basin having the saddle landform.

Also, it is known that in 2015, there occurred a heavy flood along the basin, it can be seen that the morphometry did undergo drastic changes in the year 2009 to 2022 that the area became a complete saddle landform compared to the change that was obtained from 1995 to 2009. This shows that sedimentation and erosion caused by floods play an important role in the formation of landforms.

5.2 Recommendation

The result obtained showed a great impact of settlement along the basin in terms of morphometric change specifically in the sese of change of landforms. One can further study the morphological dynamics in terms of hydrological modeling to see a time series changes of hydrological parameters on the basin.

REFERENCES

Ali, K., & Singh, G. P. (2022). Morphometric Analysis of Dhasan River Basin, Madhya Pradesh, India, Using Remote Sensing and Arc GIS Techniques [Research article]. *Trends in sciences 2022*, *19*(10). https://doi.org/10.48048/tis.2022.4182

Alshari, E. A., & Gawali, B. W. (2021). Development of classification system for LULC using remote sensing and GIS. In *Global Transitions Proceedings* (Vol. 2, pp. 8–17). Elsevier.

Argialas, D. P., & Miliaresis, G. C. (1997). Landform spatial knowledge acquisition: identification, comceptualization and representation. *American Society for Photogrammetry*.

Armstrong, A. M. (1987). Master Planning for Dar es Salaam, Tanzania. *Habitat International*(11), 133-145. https://doi.org/10.1016/0197-3975(87)90064-6

Barton, D., & Leonov, S. (1997). Radar technology encyclopedia. In S. Leonov (Ed.), (pp. 511). Artec House, Norwood, MA, USA.

Boussema, M. R. (2017). GIS Use for Mapping Land Degradation: A Review of Research Carried Out in Tunisia. https://doi.org/10.4018/978-1-5225-0937-0.ch003

Braun, A. (2021). Retrieval of digital elevation models from Sentinel-1 radar data – open applications, techniques, and limitations. *Open Geosciences*. https://doi.org/10.1515/geo-2020-0246

Dimyati, M., Mizuno, K., Kobayashi, S., & Kitamura, T. (1996). An analysis of land use/cover change using the combination of MSS Landsat and land use map: a case study in Yogyakarta. *Wiley & Sons*, 4439-4447.

Douglas, I., Alam, K., Maghenda, M., McDonnel, Y., McLean, L., & Campbell, J. (2008). Unjust Waters. Climate Change, Flooding and the Urban Poor in Africa. *Environment and Urbanisation*, *20*, 187-205. https://doi.org/10.1177/0956247808089156

Evans, I. S., & Cox, N. J. (1974). Geomorphometry and the operational definition of cirques. *Area*, *6*(2), 150–153.

Frost, V. S., Stiles, J. A., Holtzman, J. C., & Held, D. N. (1980). Earth Resources And Remote Sensing.

Gurnell, A., Lee, M., & Souch, C. (2007). Urban rivers: Hydrology, geomorphology, ecology and opportunities for change. *Geography Compass*, *1*(5), 1118– 1137. https://doi.org/10.1111/j.1749-8198.2007.00058.x

Igulu, B. S., & Mshiu, E. E. (2020). Monitoring Impervious Surface Area Dynamics to Assess Urbanisation of a Catchment: Msimbazi River Valley Dar es Salaam, 1989 - 2015. *Tanzania Journal of Science*.

Kalisa, D., Majule, A., & Lyimo, J. G. (2013). Role of wetlands resource utilization on community livelihoods: The case of Songwe River Basin, Tanzania. *Afr. J. Agric. Res*, *8*, 6457–6467.

Kibugu, C. P., Munishia, S., & Kongo, V. (2022). Impacts of Land Cover Change Caused by Urbanization on the Flood Regime of Msimbazi Catchment in Dar es Salaam, Tanzania. *Tanzania Journal of Engineering and Technology*, *41(2)*, 35-51.

Kironde, J. M. L. (2016). Governance Deficits in Dealing with the Plight of Dwellers of Hazardous Land: The Case of the Msimbazi River Valley in Dar es Salaam, Tanzania. *Current Urban Studies, 4*, 303-328. https://doi.org/10.4236/cus.2016.43021

Kumar, B. (2021). Image Preprocessing — Why is it Necessary? *Spider*.

Lillesand, T. M., & Keifer, R. W. (1994). Remote Sensing and Image Interpretation.

Lu, D., Mausel, P., Brondizio, E., & Moran, E. (2004). Change detection techniques. *International Journal of Remote Sensing*, *25*(12).

Lu, Z., Jung, H.-S., Zhang, L., Lee, W., Lee, C.-W., & Dzurisin, D. (2012). Digital elevation model generation from satellite interferometric synthetic aperture radar. In D. Ramsey & R. Rykhus (Eds.), *Advances in mapping from aerospace imagery*.

Machiwa, H., Mango, J., Sengupta, D., & Zhou, Y. (2021). Using Time-Series Remote Sensing Images in Monitoring the Spatial–Temporal Dynamics of LULC in the Msimbazi Basin, Tanzania. *Land*, *10,1139*.

Marrakchi, O. C., Charfi, C. M., Hamzaoui, M., & Habaieb, H. (2021). Improvement of Sentinel-1 Remote Sensing Data Classification by DWT and PCA. *Journal of Sensors*, 12, Article 8897303. https://doi.org/10.1155/2021/8897303

Mascolo, L., Lopez-Sanchez, J. M., & Cloude, S. R. (2021). Thermal Noise Removal From Polarimetric Sentinel-1 Data. *IEEE Geoscience And Remote Sensing Letters*.

Massonnet, D., Rossi, M., Carmona, C., Adragna, F., Peltzer, G., Feigl, K., & T.Rabaute. (1993). The displacement field of Landers earthquake mapped bby radar interferometry. *Nature, 3646433*, 138-142.

Nelson, J. (2020). What is Image Preprocessing and Augmentation? *Roboflow*.

Pike, R. J., Böhner, J., Dobos, E., Emeis, S., Evans, I. S., Gessler, P., Gruber, S., Guth, P. L., Hengl, T., Hofierka, J., Jelaska, S. D., Lindsay, J., MacMillan, R. A., Nelson, A., Ferrero, V. O., Peckham, S. D., Reuter, H. I., Temme, A., & Wood, J. (2009). *GEOMORPHOMETRY Concepts, Software, Applications* (T. Hengl & H. I. Reuter, Eds. Vol. 33). Elsevier.

PO-RALG. (2021). *The Msimbazi development project*. T. U. R. O. Tanzania.

Satpalda. (2018). Significance of Land Use / Land Cover (LULC) Maps.

Shary, P. A. (1995). Land surface in gravity points classification by a complete system of curvatures. *Mathematical Geology*, *27*(3), 373–390.

Straumann, R. (2010). *Extraction and characterisation of landforms from digital elevation models: fiat parsing the elevation field* Zurich.

Subha. (2019). Image Classification Techniques in Remote Sensing. *Agira Innovation Engineered*.

Sukeshini, N. A., Reddy, G. P. O., & Kumaraswamy, K. (2020). Automatic Extraction of Landforms in a Complex Terrain of Western Ghats Region of India Using Earth Observation Datasets and GIS. *Asian Association on Remote Sensing*.

Thorn, C. E. (1988). An Introduction to Theoretical Geomorphology. *Unwin Hyman*, 247.

Tobler, W. R. (2000). The development of analytical cartography — a personal note. *Cartography and Geographic Information Science*, *27*(3), 189–194.

Utepov, Y., Aniskin, A., Mkilima, T., Shakhmov, Z., & Kozina, G. (2020). Potential Impact of Land-Use Changes on River Basin Hydraulic Parameters Subjected to Rapid Urbanization. *Tehnički vjesnik*, 1519-1525. https://doi.org/10.17559/TV-20200808134641

Wang, Q., Liu, S., Chanussot, J., & X. Li. (2019). Scene classification with recurrent attention of vhr remote sensing images. *IEEE Transactions on Geoscience and Remote Sensing*, *57*, 1155–1167.

Wang, Y. Q., Damon, C., Archetto, G., Robadue, D., & Fenn, M. (2012). Land Cover Mapping of the Greater Cape Three Points Area Using Landsat Remote Sensing Data. Coastal Resources Center, University of Rhode Island. . *USAID Integrated Coastal and Fisheries Governance Program for the Western Region of Ghana*, 48 pp.

Woodhouse, J. (2018). Geomorphology support for the city of Dar es Salaam. *JBA consulting*.

Yu, J. H., & Ge, L. (2010). Digital Elevation Model generation using ascending and descending multi-baseline ALOS/PALSAR radar images. *Remote Sensing and Imagery II*.